Received: 11 September 2019 | Revised: 5 September 2020 | Accepted: 7 September 2020

DOI: 10.1111/pce.13891

ORIGINAL ARTICLE

Plant, Cell & Environment

WILEY

Wood day capacitance is related to water content, wood density, and anatomy across 30 temperate tree species

Kasia Ziemińska[1,2] | Emily Rosa[3] | Sean M. Gleason[4] | N. Michele Holbrook[5]

[1]Arnold Arboretum of Harvard University, Boston, Massachusetts

[2]Department of Plant Ecology and Evolution, Uppsala University, Uppsala, Sweden

[3]Department of Biology, Sonoma State University, Rohnert Park, California

[4]United States Department of Agriculture – Agricultural Research Service, Water Management and Systems Research Unit, Fort Collins, Colorado

[5]Department of Organismic and Evolutionary Biology, Harvard University, Cambridge, Massachusetts

Correspondence
Kasia Ziemińska, Department of Plant Ecology and Evolution, Evolutionary Biology Centre, Uppsala University, Norbyvägen 18D, 752 36 Uppsala, Sweden.
Email: kasia.s.zieminska@gmail.com

Funding information
The Arnold Arboretum of Harvard University through DaRin Butz Foundation Research Internship; The Arnold Arboretum of Harvard University through Postdoctoral Putnam Fellowship

Abstract

Water released from wood during transpiration (capacitance) can meaningfully affect daily water use and drought response. To provide context for better understanding of capacitance mechanisms, we investigated links between capacitance and wood anatomy. On twigs of 30 temperate angiosperm tree species, we measured day capacitance (between predawn and midday), water content, wood density, and anatomical traits, that is, vessel dimensions, tissue fractions, and vessel–tissue contact fractions (fraction of vessel circumference in contact with other tissues). Across all species, wood density (WD) and predawn lumen volumetric water content ($VWC_{L\text{-}pd}$) together were the strongest predictors of day capacitance (r^2_{adj} = .44). Vessel–tissue contact fractions explained an additional ~10% of the variation in day capacitance. Regression models were not improved by including tissue lumen fractions. Among diffuse-porous species, $VWC_{L\text{-}pd}$ and vessel–ray contact fraction together were the best predictors of day capacitance, whereas among semi/ring-porous species, $VWC_{L\text{-}pd}$, WD and vessel–fibre contact fraction were the best predictors. At predawn, wood was less than fully saturated for all species (lumen relative water content = 0.52 ± 0.17). Our findings imply that day capacitance depends on the amount of stored water, tissue connectivity and the bulk wood properties arising from WD (e.g., elasticity), rather than the fraction of any particular tissue.

KEYWORDS

angiosperm trees, fibres, parenchyma, vessels, water storage, wood anatomy

1 | INTRODUCTION

Water stored in wood can buffer excessive evaporative demand on diurnal (Carrasco et al., 2015; Goldstein et al., 1998; Köcher, Horna, & Leuschner, 2013; Lachenbruch & McCulloh, 2014; Meinzer et al., 2008; Meinzer, James, & Goldstein, 2004; Meinzer, Johnson, Lachenbruch, McCulloh, & Woodruff, 2009; F. G. Scholz et al., 2007) and seasonal time scales (Hao, Wheeler, Holbrook, & Goldstein, 2013; Pratt & Jacobsen, 2017; Salomón, Limousin, Ourcival, Rodríguez-Calcerrada, & Steppe, 2017). Estimates of the contribution of stored water to a tree's daily water budget range from 5 to 50% (Carrasco et al., 2015; Goldstein et al., 1998; Kobayashi & Tanaka, 2001; Köcher et al., 2013; Meinzer et al., 2004; Phillips et al., 2003; F. G. Scholz et al., 2007). Thus, water storage can be an important component of whole-plant water balance (Blackman et al., 2016; Christoffersen et al., 2016; Gleason, Blackman, Cook, Laws, & Westoby, 2014). However, the mechanisms of water storage and release, and their structural underpinnings remain unclear. Consequently, our understanding of cost vs. benefits of water storage and how storage is coordinated with other tree functions is limited. Here, our objective was to quantify water storage (amount of stored water) and day capacitance (water released per wood volume per change in stem water potential between predawn and midday, kg m^{-3} MPa^{-1}) across a diverse suite of 30 temperate angiosperm trees.

Wood capacitance is most often measured using psychrometers and estimated as the initial slope extracted from a water release–water potential curve (Jupa, Plavcová, Gloser, & Jansen, 2016; McCulloh et al., 2012; Meinzer et al., 2008; Meinzer, James,

Goldstein, & Woodruff, 2003; Santiago et al., 2018; F. G. Scholz et al., 2007; Siddiq, Zhang, Zhu, & Cao, 2019; Trifilò et al., 2015). However, if tissues *in natura* never become fully saturated, or if the operating water potential of xylem falls outside the initial water release curve, then this way of estimating capacitance may be functionally irrelevant. Oversaturating wood prior to measuring capacitance may also skew results. Moreover, using psychrometers on excised material likely results in water being released from the cut ends of "open" vessels, rather than from tissues that store and release water in intact wood (Jupa et al., 2016; Tyree & Yang, 1990). Few studies have estimated day capacitance across the range of water potentials experienced by field plants, with only two studies using pressure chamber measurements of non-transpiring leaves (Wolfe & Kursar, 2015; Zhang, Meinzer, Qi, Goldstein, & Cao, 2013) and one study using psychrometers on excised tissues (Richards, Wright, Lenz, & Zanne, 2014). We addressed this shortcoming by measuring capacitance between predawn and midday during peak summer conditions. To avoid open vessels and oversaturation artefacts, we estimated capacitance from the difference in wood water content between predawn and midday with the corresponding change in stem water potential measured using bagged, non-transpiring (equilibrated) leaves (Begg & Turner, 1970; Clearwater & Meinzer, 2001). We refer to this measure as "day capacitance," following Zhang et al. (2013).

Anatomical structure should determine wood capacitance (Holbrook, 1995; Tyree & Yang, 1990; Zimmermann, 1983). Tyree and Yang (1990) proposed that water release consists of three phases linked to anatomy: (a) an initial phase (0 to ca. −0.6 MPa), when water is released from capillary storage (already embolized fibres, vessels and tracheids, and intercellular spaces), (b) a second phase (< −0.6 MPa but prior to vessel embolization), when water is released from elastic storage (cells with elastic cell walls) and (c) a final phase (below the embolization threshold), when water is released from embolizing vessels and fibres, likely resulting in permanent damage to the water transport in xylem tissue, at least in large trees. Despite this well-developed and popular theory, few studies have quantified wood anatomy in relation to capacitance, and none of them used methods which would avoid open vessels and oversaturation artefacts. As a result, we lack quantitative understanding of the anatomical drivers of capacitance, especially for angiosperm trees, which exhibit substantial variation in stem cell sizes, types, their proportions and geometry.

Given these knowledge gaps, it is surprising that parenchyma, the main living tissue in wood commonly believed to have elastic cell walls, is often assumed the primary source of capacitance in stems of angiosperm trees (e.g., Li et al., 2018; Meinzer et al., 2003; Morris et al., 2016; Plavcová & Jansen, 2015; Rungwattana & Hietz, 2018; Santiago et al., 2018; Steppe & Lemeur, 2007; Vergeynst, Dierick, Bogaerts, Cnudde, & Steppe, 2015). Several studies have extended this idea to suggest that a higher parenchyma fraction may therefore confer higher capacitance (Borchert & Pockman, 2005; Nardini, Savi, Trifilò, & Lo Gullo, 2018; Pratt & Jacobsen, 2017; F. G. Scholz, Phillips, Bucci, Meinzer, & Goldstein, 2011; Secchi, Pagliarani, & Zwieniecki, 2017). While this may indeed be the case in highly parenchymatous stems like palms or baobabs (Chapotin, Razanameharizaka, & Holbrook, 2006a, 2006b; Holbrook & Sinclair, 1992), it may be less probable for the majority of angiosperm tree species, which tend to have lower wood parenchyma fractions (Morris et al., 2016). In these species, parenchyma cells are connected with other cells (fibres, vessels and—in some taxa—tracheids) via highly lignified middle lamellae that likely impede parenchyma from the independent expansion and contraction. Moreover, recent microCT studies suggest that water released from cavitating fibres and vessels may contribute meaningfully to capacitance at moderate water potentials (Knipfer et al., 2017, 2019; Yazaki et al., 2020). If the cavitation of cell lumens rather than elastic shrinkage of living tissues is responsible for the release of capacitance water, we should then expect capacitance to be linked to fibre and/or vessel lumen fractions, rather than parenchyma.

Vessel diameter distribution has traditionally been used to categorize the wood of temperate tree species: diffuse-porous, semi-ring-porous and ring-porous ("porous" refers to a "pore" which denotes a "vessel," IAWA Committee, 1989). Diffuse-porous species have vessels of similar size that are distributed "diffusely" (i.e., evenly) across their growth rings. Ring-porous species have relatively large vessels concentrated in a "ring" within the earlywood and considerably smaller vessels in the latewood. Semi-ring-porous species exhibit vessel characteristics somewhere in between these two categories. This spectrum of anatomies is unique to temperate species, while tropical woods typically display diffuse-porous structure and, usually, lack annual growth rings. Vessels aside, it remains uncertain if and how other anatomical features differ between the porosity types and what consequences they may have on capacitance and other wood functions across a varied set of species (but see Jupa et al., 2016). To better understand the scope of anatomical variation and the linkages between anatomy and capacitance, we selected anatomically-diverse species set that represented the entire porosity spectrum.

Here, we measured detailed anatomical traits, water storage and day capacitance across 30 temperate angiosperm tree species to address two main questions: (a) what is the magnitude and range of day capacitance and wood water content across species *in natura*? and (b) are particular anatomical features associated with these two traits?

2 | MATERIALS AND METHODS

2.1 | Site, species and individuals

All measurements were taken from trees growing at the Arnold Arboretum of Harvard University in Boston, Massachusetts, USA. Mean annual temperature (MAT) in 2017, the year when day capacitance measurements were taken, was 10.9°C and annual precipitation (AP) was 787 mm. From 2013 to 2019 (for which detailed climate

data was available), average MAT was 10.8°C and average AP was 1,000 mm, indicating that 2017 was a relatively dry year. Mean temperature during sampling (August) was 21.2°C and precipitation was 22 mm. Temperature and precipitation throughout the year preceding measurements is shown in the Supporting Information (Figure S1 in Data S1). Soil texture is variable across the Arboretum and sampled trees grew on: sandy loam, slit loam, loamy sand, and an outcrop complex.

Thirty species of deciduous, angiosperm trees were selected, spanning 30 genera and 26 families (Table 1; tree accession numbers are listed in Table S1 in Data S1), and encompassing a broad diversity of anatomies (InsideWood, 2004; E. A. Wheeler, 2011). Due to the limited number of individuals per species, trees were sampled across the existing variation in topography and soil texture. Trees growing near streams and ponds were avoided and only healthy trees were sampled. To minimize within-species variation, trees of similar height were chosen (mean across all trees: 14 m, range: 7–25 m). Although we measured branches exposed to the midday sun, it is likely that some branches received more daily radiation than others.

2.2 | Capacitance and water storage: Sampling and measurements

Water storage and day capacitance measurements were performed during the second half of August 2017. Ten individuals per day were sampled, resulting in a total of nine sampling days. In the case of rain, sampling was delayed for 1 or 2 days. For stem water potential, leaves were enclosed in 4 mil thick, opaque, silver zip-lock bags the evening before sampling. In principle, the water potential of a bagged, non-transpiring leaf will come into equilibrium with the stem water potential. As such, bagged leaf water potential (i.e., after

TABLE 1 List of families, species, porosity types and abbreviations

Family	Species	Abbr.	Porosity	Abbr.
Sapindaceae	*Acer saccharum*	ace	Diffuse	D
Sapindaceae	*Aesculus turbinata*	aes	Diffuse	D
Betulaceae	*Betula dahurica*	bet	Diffuse	D
Cercidiphyllaceae	*Cercidiphyllum japonicum*	cer	Diffuse	D
Cornaceae	*Cornus kousa*	cor	Diffuse	D
Eucommiaceae	*Eucommia ulmoides*	euc	Diffuse	D
Fagaceae	*Fagus grandifolia*	fag	Diffuse	D
Altingiaceae	*Liquidambar styraciflua*	liq	Diffuse	D
Magnoliaceae	*Liriodendron tulipifera*	lir	Diffuse	D
Magnoliaceae	*Magnolia cylindrica*	mag	Diffuse	D
Ericaceae	*Oxydendrum arboreum*	oxy	Diffuse	D
Theaceae	*Stewartia pseudocamellia*	ste	Diffuse	D
Styracaceae	*Styrax obassia*	sty	Diffuse	D
Tiliaceae	*Tilia japonica*	til	Diffuse	D
Fabaceae	*Albizia julibrissin*	alb	Semi-ring	S/R
Bignoniaceae	*Catalpa speciosa*	cat	Semi-ring	S/R
Fabaceae	*Cladrastis kentukea*	cla	Semi-ring	S/R
Ebenaceae	*Diospyros virginiana*	dio	Semi-ring	S/R
Fabaceae	*Gleditsia triacanthos*	gle	Semi-ring	S/R
Scrophulariaceae	*Paulownia tomentosa* var. “Coreana”	pau	Semi-ring	S/R
Juglandaceae	*Carya laciniosa*	car	Ring	S/R
Oleaceae	*Fraxinus angustifolia* subsp. *oxycarpa*	fra	Ring	S/R
Moraceae	*Maclura pomifera*	mac	Ring	S/R
Moraceae	*Morus alba*	mor	Ring	S/R
Rutaceae	*Phellodendron amurense*	phe	Ring	S/R
Simaroubaceae	*Picrasma quassioides*	pic	Ring	S/R
Fagaceae	*Quercus muehlenbergii*	que	Ring	S/R
Lauraceae	*Sassafras albidum*	sas	Ring	S/R
Rutaceae	*Tetradium daniellii*	tet	Ring	S/R
Ulmaceae	*Zelkova sinica*	zel	Ring	S/R

equilibration) provides an estimate of stem water potential (Begg & Turner, 1970; Clearwater & Meinzer, 2001). Two leaves at predawn and two leaves at midday were collected. For wood water content measurements, three terminal, 0.5–0.7 m long twigs were collected at predawn and three at midday, per tree. The sampled twigs included the leaves bagged the previous evening. Twigs for each predawn-midday pair were located near each other, as close as tree architecture allowed (usually within 0.5 m), to limit the variation in water potential and water content resulting from differences in path length, height, and exposure to radiation. After collecting the predawn twig, the cut surface on the branch still attached to a tree was covered with Vaseline to reduce drying from the exposed surface. Twigs were quickly de-leafed and double-bagged in zip-lock bags. Each sampling event took approximately 2 hr. After collecting all leaves and twigs, material was transported to the onsite laboratory within 5 min.

Immediately after arrival to the laboratory, leaf water potential was measured on one leaf per tree using a pressure chamber (Model 1,000, PMS Instrument Company, USA). Next, twig segments ca. 60 mm long and 5 mm diameter (excluding bark and pith) were cut at a minimum 50 mm distance from the initial, field cut. The segments were quickly wrapped in Parafilm and placed in a 4 mil zip-lock bag. After preparing all samples, the following steps were carried out in a humidity-controlled room (at relative humidity of 75–80%) to minimize water loss. Bark and pith were removed, the ends were trimmed by a few mm, and fresh mass was measured on an analytical balance (0.00001 g), after which the samples were placed in distilled water.

These wood samples were then stored at 4°C for 2 weeks and, afterwards, saturated mass and volume was measured using Archimedes principle as described in (Ziemińska, Westoby, & Wright, 2015). For logistic reasons, we were unable to measure volume within 48 hours after sampling, however, across all species studied, volume measured on fresh vs. saturated samples (after 2 weeks of soaking at 4°C) differed on average by 2% ± 1.1% *SD*, and as such, should not meaningfully influence our volume estimates. After saturated mass and volume measurements, the samples were dried at 102°C for 3 days and dry mass was recorded.

Water storage is defined here as the amount of water contained in a wood sample. It can be expressed as two distinct indices: relative water content (RWC) and volumetric water content (VWC). RWC is the proportion of water in a sample relative to the maximum amount of water that could be stored in that sample and was calculated as follows:

$$RWC = \frac{M_F - M_D}{M_S - M_D},$$

where M_F is sample fresh mass, M_D is sample dry mass, and M_S is sample saturated mass. RWC values can range from 0 to 1, where 0 indicates a completely empty storage volume and 1 indicates an entirely full storage volume. RWC is a relative index and it does not measure how much water is stored in absolute terms.

VWC indicates total water volume per sample volume (Gartner, Moore, & Gardiner, 2004) and was calculated as follows:

$$VWC = \frac{(M_F - M_{D)}) \times \rho^{-1}}{V},$$

where ρ is water density, assumed to equal 1 g cm^{-3} and V is sample volume. Theoretically, VWC ranges from 0 to 1, where 0 indicates that there is no water in a sample and 1 indicates that the entire sample is comprised of only water. Given that wood contains cell wall, VWC values can never be 1. We calculated VWC because this measurement is directly comparable to the tissue fractions measured here. For example, a VWC of 0.5 relates to a tissue fraction also of 0.5.

Because water can be present in both cell lumen and wall, and water in cell lumen is presumably more relevant for day capacitance, we partitioned VWC to lumen (VWC_L) and wall (VWC_W) water content. To do this, we assumed that the fibre saturation point (FSP), defined as the point where only water bound in cell wall is present, is at 30% moisture content (MC, Ross, 2010; Dlouhá, Alméras, Beauchêne, Clair, & Fournier, 2018). We used a standard equation for MC:

$$MC = \frac{M_F - M_D}{M_D} \times 100\%$$

(Ross, 2010). When moisture content equals 30%, M_F becomes mass of the sample at fibre saturation point (M_{FSP}):

$$30\% = \frac{M_{FSP} - M_D}{M_D} \times 100\%,$$

which then can be estimated as follows:

$$M_{FSP} = 1.3 \times M_D.$$

We then substituted M_{FSP} into the VWC equation (defined above) to estimate the VWC_L:

$$VWC_L = \frac{(M_F - M_{FSP}) \times \rho^{-1}}{V}$$

and for cell wall:

$$VWC_W = \frac{(M_{FSP} - M_D) \times \rho^{-1}}{V}.$$

Next, we estimated the lumen relative water content (RWC_L, Longuetaud et al., 2016):

$$RWC_L = \frac{M_F - M_{FSP}}{M_S - M_{FSP}}.$$

All water content indices were estimated at predawn and midday, indicated by subscripts “pd” and “md,” respectively.

Following a simplified version of the equation from Meinzer et al. (2003) and Richards et al. (2014), cumulative water released (CWR, kg m^{-3}) was calculated, separately for predawn and midday, as follows:

$$CWR = \frac{M_S - M_F}{V},$$

where V is sample volume, and then multiplied by 1,000 to convert the units from g cm^{-3} to kg m^{-3}. Wood day capacitance (kg m^{-3} MPa^{-1}) was estimated as:

$$Day\ capacitane = \frac{CWR_{md} - CWR_{pd}}{\psi_{pd} - \psi_{md}},$$

where Ψ is stem water potential, and subscripts indicate predawn ('pd') and midday ('md'). This calculation of day capacitance takes saturation as a reference point, to minimize the effect of intrinsic differences between predawn and midday samples (e.g., in their wood density). An alternative equation for calculation of day capacitance is discussed in Supporting Information (Notes S1, Figure S2 in Data S1).

All measured traits, their abbreviations and units are listed in Table 2.

TABLE 2 Measured traits, abbreviations and units

Trait	Abbr	Units
Day capacitance		kg m^{-3} MPa^{-1}
Cumulative water released	CWR_{pd}, CWR_{md}, $\Delta CWR_{md\text{-}pd}$	kg m^{-3}
Stem water potential	Ψ_{pd}, Ψ_{md}, $\Delta\Psi_{pd\text{-}md}$	MPa
Volumetric water content	VWC_{pd}, VWC_{md}, $\Delta VWC_{pd\text{-}md}$	Unitless
Volumetric water content: Saturated	VWC_{sat}	"
Lumen volumetric water content	$VWC_{L\text{-}pd}$, $VWC_{L\text{-}md}$, $\Delta VWC_{L\text{-}pd\text{-}md}$	"
Lumen volumetric water content: Saturated	$VWC_{L\text{-}sat}$	"
Wall volumetric water content	VWC_{W}	"
Relative water content	RWC_{pd}, RWC_{md}, $\Delta RWC_{pd\text{-}md}$	"
Lumen relative water content	$RWC_{L\text{-}pd}$, $RWC_{L\text{-}md}$, $\Delta RWC_{L\text{-}pd\text{-}md}$	"
Wood density	WD	g cm^{-3}
Fibre fraction: w, l		Unitless
Axial+ray parenchyma fraction: w, l		"
Axial parenchyma fraction: w, l		"
Ray fraction: w, l		"
Vessel fraction: w, l		"
Living fibre fraction: w + l		"
$Conduits_{15}$ fraction: w + l		"
Vessel–fibre contact fraction		"
Vessel–axial+ray parenchyma contact fraction		"
Vessel–axial parenchyma contact fraction		"
Vessel–ray contact fraction		"
Vessel–vessel contact fraction		"
Vessel–living fibre contact fraction		"
Vessel–$conduits_{15}$ contact fraction		"
Vessel mean area		μm^2
Vessel mean diameter		μm
Hydraulically weighted vessel diameter	D_H	"
Vessel number per area		mm^{-2}
Vessel size to number ratio		mm^4
Lumen and wall fraction per given tissue	For example, $lumen\ fraction_{fibre}$, $wall\ fraction_{fibre}$	Unitless

Note: Fractions of wall (w), lumen (l) and wall + lumen (w + l) of a given tissue were measured. Subscripts denote: lumen (L), predawn (pd), midday (md) and difference between predawn and midday (pd-md).

2.3 | Anatomy: Sampling and measurements

For anatomical measurements, one, midday sun-exposed twig per tree was collected in August 2016. Twigs were transported to the lab and stored in 70% ethanol for 3 months until further processing. In about a third of cases, samples collected in 2016 and 2017 were taken from different individuals (Table S1 in Data S1) due to either deteriorated tree health or storm damage. Twig size (diameter and length) and location on the tree were consistent between 2016 and 2017 sampling, although in some cases slightly lower branches were measured in 2017 to allow for leaf bagging.

Cross-sections ~10–20 μm thick were made using a Reichert sledge microtome, stained in a mixture of safranin O and Alcian Blue (0.35 g safranin O in 35 ml 50% ethanol +0.65 g of Alcian Blue in 65 ml of distilled water) and mounted in glycerol. Longitudinal radial and tangential sections of one sample per species were also taken to assist in anatomical interpretations. Several photos of a pie-shaped region stretching from pith to cambium were taken using a 20x objective, Zeiss Axiophot microscope and AxioCam 512 camera (ZEISS, Germany). The photos were then stitched together in Image Composite Editor.

Anatomical measurements were done on one cross-section per individual, three individuals per species (Table S1 in Data S1), across all growth rings (4.4 ± 1.5 *SD*). Only vessel–tissue contact fractions (see below) were measured on all except the innermost ring due to the substantial time/labour cost of this measurement. The potential error resulting from this approach is likely minimal. Our tests on a subset of samples indicated that fractions measured on all growth rings were strongly correlated with fractions measured on all except innermost ring (r^2 > .9 for most tissues). All samples exhibited a clear porosity pattern typical for a given species, except for the innermost growth ring of ring-porous species, which often displayed a semi-ring- or diffuse-porous anatomy.

Lumen and wall tissue fractions were measured for all major tissues: fibre, axial parenchyma, ray parenchyma and vessels. From these measurements, we also calculated the fraction of lumen and wall per given tissue. Conduits with maximum diameter <15 μm—denoted hereafter "conduits$_{15}$"—were also recorded. Conduits$_{15}$ likely included small vessels, the tapered ends of vessels (tails), and tracheids. Living fibres were identified by the presence of starch, nuclei or septa, and their wall thickness was similar to fibres and/or thicker than parenchyma walls. For conduits$_{15}$ and living fibres, the fractions of lumen and wall were counted together. The vessel characteristics measured included: vessel mean area and diameter (mean of minimum and maximum diameters of a given vessel), hydraulically weighed diameter (D_H = Σdiameter^5 / Σdiameter^4; Sperry, Nichols, Sullivan, & Eastlack, 1994), vessel number per cross-sectional area, and the vessel size-to-number ratio (mean vessel area divided by vessel number per cross-sectional area). We also measured the proportion of vessel circumference in contact with other tissues, referred to collectively as "vessel–tissue contact fraction." For example, "vessel–axial parenchyma contact fraction" is the proportion of vessel circumference in contact with axial parenchyma.

All vessels, excluding protoxylem, were coloured in GIMP (www.gimp.org) and measured in ImageJ (Schneider, Rasband, & Eliceiri, 2012). Images were processed using Wacom Cintiq 22HD pen display (Wacom Technology Corporation, Portland, USA).

For tissue fractions, a grid method was applied. A grid point matrix was laid over the pie region in ImageJ and was classified using a "Cell counter" plugin depending on which tissue each point fell onto (figure 1 in Ziemińska et al., 2015). The distance between grid points was 55 μm. On average, we analysed 484 (± 128) points per pie region. For ray wall fraction we counted only walls perpendicular to the cross-section plane, and as such our measurements are likely underestimates. The features attributable to living fibres (starch, nuclei and septa) were not always visible within each cross-section, and hence, our measurements of living fibre fractions may have been underestimated as well. For vessel–tissue contact fractions, all vessels in a pie region were analysed except for the innermost growth ring (see above). In Photoshop, dots were placed at equal distances to each other at 22.5 μm along the vessel lumen circumference (Figure 1; the distance between the first and last dot varied as a result of variable circumference, and the last dot was counted only when its distance to the first dot was larger than 11 μm). Next, using the "Cell counter" plugin, we classified each dot depending on the neighbouring tissue. For instance, if the dot fell on the border with ray, it was classified as vessel–ray contact dot. We then took the ratio of all vessel–ray

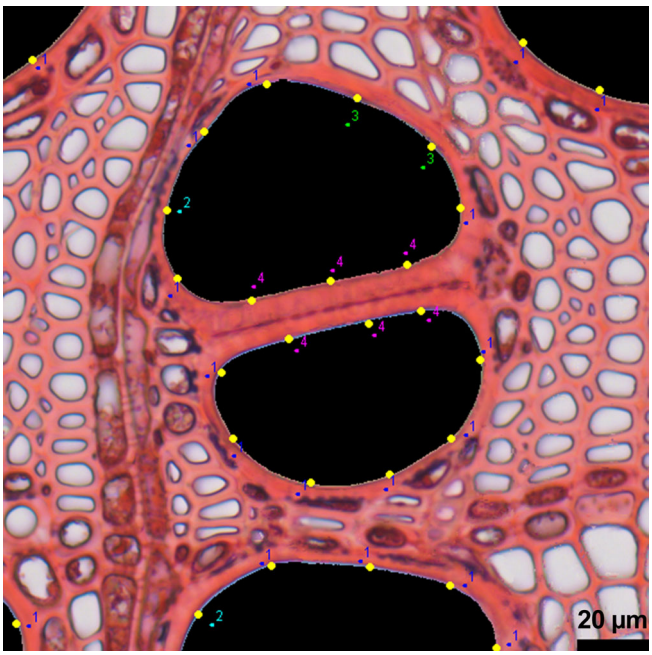

FIGURE 1 Illustration of the method used to estimate vessel–tissue contact fractions between vessels and other tissues (fibres, axial parenchyma, rays, vessels, living fibres, conduits$_{15}$). The image shows a fragment of a cross-section of *Fraxinus angustifolia* subsp. *oxycarpa*. Yellow dots distributed on a vessel (black) circumference are classified based on the tissue in contact with a vessel (1 – axial parenchyma, 2 – rays, 3 – fibres, 4 – vessels, not shown: conduits$_{15}$ and living fibres) [Colour figure can be viewed at wileyonlinelibrary.com]

contact dots to total analysed dots in each pie region, and did the same for the other tissues. This "dot-ratio" is therefore the vessel–tissue contact fraction for each abutting tissue. On average, we analysed 943 dots (±605) per each pie region.

2.4 | Wood density

Basic wood density, hereafter "wood density" (WD) for brevity, was measured on the same samples as water storage and day capacitance measurements, and was calculated as dry mass divided by saturated volume (g cm^{-3}).

2.5 | Data analysis

The studied species encompassed 14 diffuse-porous, 10 ring-porous, and 6 semi-ring-porous species. Preliminary data analysis showed considerable anatomical differences, not only in vessel size, as might be expected, but also in tissue fractions and vessel–tissue contact fractions. Anatomically, diffuse-porous species were very different from ring-porous and semi-ring-porous species, which in turn were similar to each other (Figure S3 in Data S1). Moreover, many of the ring-porous and semi-ring-porous species occur in both forms (InsideWood, 2004). Consequently, we grouped ring-porous and semi-ring-porous into one category, denoted hereafter as "semi/ring-porous." All analyses were run within as well as across porosity groups.

Statistical analyses were performed in R (R Core Team, 2018). We used linear bivariate and multiple regression models to assess predictors of day capacitance using the "lm" function. The distribution of residuals was evaluated using the "residualPlot" and "qqPlot" functions in the "car" package (Fox & Weisberg, 2011). Our modelling approach was as follows: (a) firstly, we analysed bivariate relationships between capacitance (response variable) and a set of predictors (wood density, $VWC_{L\text{-}pd}$, $RWC_{L\text{-}pd}$, vessel average area and hydraulically weighted diameter, all tissue lumen fractions and all vessel–tissue contact fractions. (b) secondly, we built multiple regression models that contained the two strongest predictors of capacitance, (c) To assess the potential influence of anatomical features in addition to WD and $VWC_{L\text{-}pd}$, we built five multiple regression models of the following structure: (a) $VWC_{L\text{-}pd}$ + WD + tissue fraction, (b) $VWC_{L\text{-}pd}$ + WD + contact fraction, (c) $VWC_{L\text{-}pd}$ + tissue fraction, (d) $VWC_{L\text{-}pd}$ + contact fraction and (e) $VWC_{L\text{-}pd}$ + tissue fraction + contact fraction. We repeated these steps three times: across all species, diffuse-porous and semi/ring-porous. However, to avoid over-fitting, within-porosity group models contained a maximum of two predictors. We selected the three best models based on r^2 (bivariate) or r^2_{adj} (multiple) values. Anatomical traits analysed in the multiple models included lumen fractions of fibre, vessel, axial parenchyma, ray parenchyma, and axial+ray parenchyma, and contact fractions of vessel–fibre, vessel–vessel, vessel–axial parenchyma, vessel–ray parenchyma, vessel–axial+ray parenchyma. Collinearity of predictors was assessed using the variance inflation factor (VIF, "vif" function). When VIF > 4, we removed the variables from the model (Kabacoff, 2015). Correlation matrices were obtained using the "corrplot" function in "corrplot" package (Wei & Simko, 2017), and scatterplot matrices were obtained using the "pairs" function. For all regression models and correlation analyses, we removed *Paulownia tomentosa* because due to its exceptionally high capacitance, it was often an outlier (see Results and Figures).

3 | RESULTS

3.1 | Hydraulic traits: Day capacitance, water storage, cumulative water released and stem water potential

Day capacitance was on average 53 ± 26 (mean ± one *SD*) kg m^{-3} MPa^{-1}, excluding *P. tomentosa*, and ranged from 8 to 99 kg m^{-3} MPa^{-1}. The outlier, *P. tomentosa*, had a day capacitance of 505 kg m^{-3} MPa^{-1}. In comparison with other studied species, *P. tomentosa* leafed out the latest (late May/early June; up to 2 months after the early leaf flushing species) and had the largest pith water volume. These factors likely contributed to the observed high water content (Figure 2a), low $\Delta\Psi_{pd\text{-}md}$ (0.13 MPa), and exceptionally high capacitance for this species.

The amount of water released between predawn and midday ($\Delta CWR_{pd\text{-}md}$) was on average 37 ± 14 kg per m^3 of wood (range: 11 to 69 kg m^{-3}). Mean predawn stem water potential (Ψ_{pd}) was −0.46 MPa and ranged from −0.21 to −0.93 MPa. Mean midday stem water potential (Ψ_{md}) was −1.22 MPa and ranged from −0.37 to −2.1 MPa. The largest change between predawn and midday water potentials ($\Delta\Psi_{pd\text{-}md}$) was 1.6 MPa and the smallest was 0.13 MPa. Table S2 in Data S1 lists summary statistics for all measured traits.

Mean lumen volumetric water content (VWC_L), which indicates the fraction of wood volume that is occupied by water in cell lumen, was 0.25 ± 0.09 at predawn, 0.21 ± 0.08 at midday and 0.47 ± 0.09 at saturation (Table S2 in Data S1, Figure 2a). Mean wall VWC (VWC_W) was 0.16 ± 0.03 and was positively correlated with total wall fraction (r^2 = .62, p < .001). Lumen relative water content (RWC_L) was 0.52 ± 0.17 at predawn and 0.45 ± 0.16 at midday, meaning that about half of cell lumen volume was occupied by water (Figure 2b), and half was devoid of it. Results for total (wall+lumen) VWC and RWC are reported in Supporting Information (Table S2, Figure S4 in Data S1). Predawn water content was strongly associated with midday water content for all water content indices (r^2 > .97, p < .001), therefore, we hereafter report predawn measurements only.

Tissue lumen fractions and VWC_L are directly comparable to each other because they both express the proportion of wood volume that is taken up by cell lumen or water in lumen. Therefore, total lumen fraction (lumen fraction for all tissues) should be correlated with VWC_L at saturation ($VWC_{L\text{-}sat}$) i.e., when all cell lumen is filled up with water. In concordance with this expectation, $VWC_{L\text{-}sat}$ was strongly correlated with total lumen fraction (r^2 = .63, p < .001, Figure S5 in

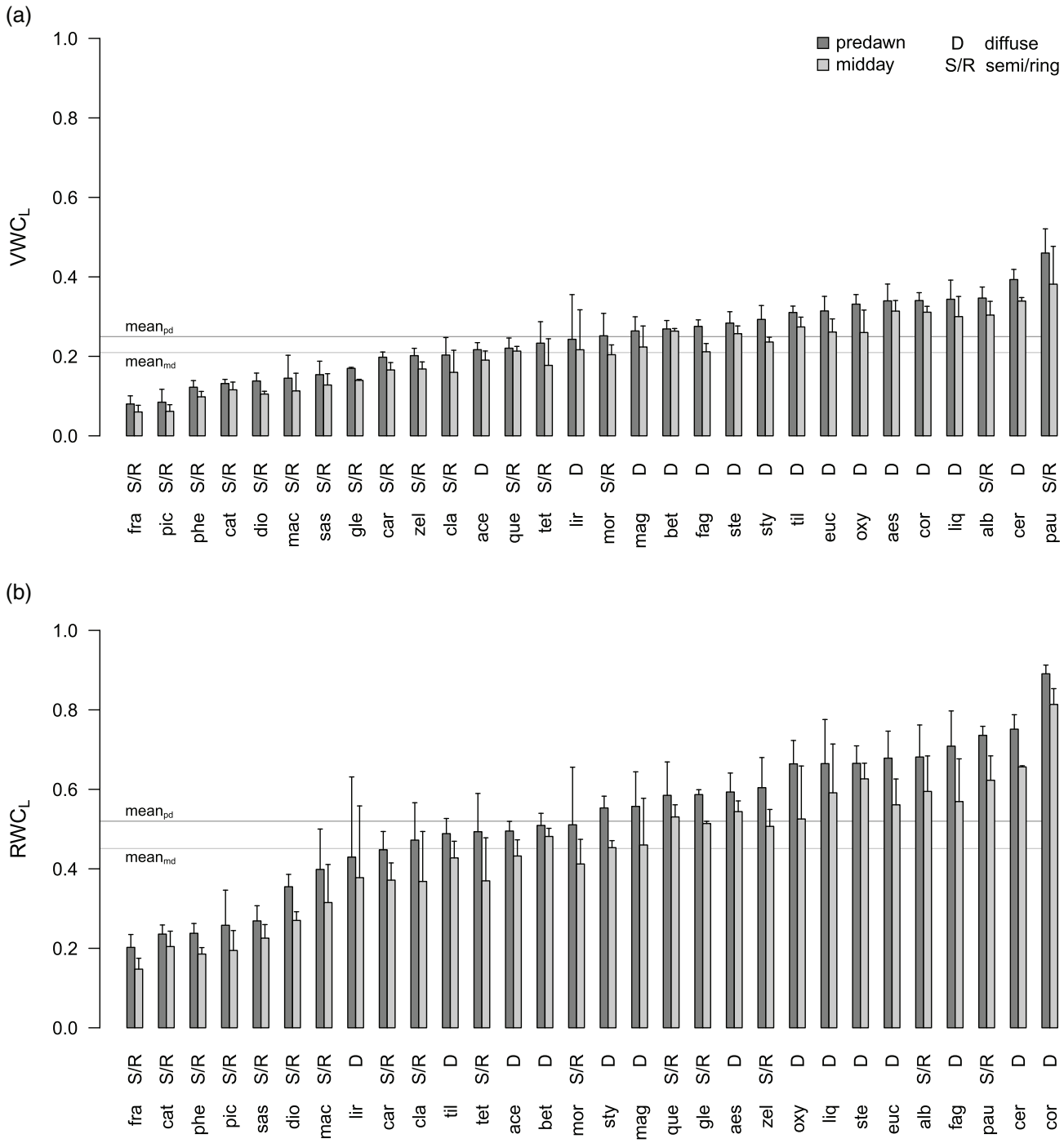

FIGURE 2 Predawn and midday lumen volumetric water content (VWC_L, a) and lumen relative water content (RWC_L, b). VWC_L is the fraction of sample volume that is occupied by water in lumen in a fresh sample and RWC_L is the ratio of water volume in lumen in a fresh sample relative to maximum amount of water volume that can be stored in lumen. Error bars denote one *SD* (n = 3). "D" denotes diffuse-porous and "S/R," semi/ring-porous species. Three-letter codes indicate different species (Table 1). Horizontal lines indicate predawn and midday mean values across all species (n = 30). Barplots showing VWC and RWC for entire wood sample (wall + lumen), instead of lumen only, are shown in Figure S4 in Data S1

Data S1). The slope of this relationship was not significantly different from 1 (p = .53, major axis fit, Warton, Duursma, Falster & Taskinen 2012) and the intercept was not significantly different from 0 (p = .29), suggesting that these two measurements—tissue fractions calculated from cross-sections and water fractions calculated from sample mass measurements—are indeed directly comparable. This result validates the analysis of tissue lumen fractions and VWC_L relationships.

3.2 | Anatomical traits: Tissue fractions, vessel–tissue contact fractions and vessels

Anatomical variation in tissue fractions, vessel–tissue contact fractions and vessel dimensions was considerable (Table S2 in Data S1, Figure 3). Fibres represented the highest fraction (0.45 ± 0.08), followed by axial+ray parenchyma (0.28 ± 0.08), and then vessels (0.24 ± 0.11). Average axial+ray parenchyma fraction was higher than that found by a previous global analysis of ~400 temperate angiosperm species (0.21) and ranged from 0.16 to 0.43, spanning nearly the entire range of variation in temperate angiosperm species, and nearly half of variation existing across angiosperm species worldwide (Morris et al., 2016). Vessel fraction encompassed almost the entire spectrum of global variation (Zanne et al., 2010). $Conduits_{15}$ were the least abundant (0.016 ± 0.023, absent in *P. tomentosa*). Living fibres were observed in eight species and comprised only a small fraction of total wood cross-sectional area (0.026 ± 0.037) with *Acer saccharum* a notable outlier (0.11).

The proportion of a given tissue that is occupied by lumen (lumen $fraction_{tissue}$) and wall (wall $fraction_{tissue}$) varied considerably across tissue types (Table S2 in Data S1, Figure 3a), with vessels exhibiting the largest lumen $fraction_{vessel}$ (0.82 ± 0.04), followed by rays (0.64 ± 0.05), axial parenchyma (0.52 ± 0.10), and fibres (0.30 ± 0.15). These results are discussed in Supporting Information (Notes S2, Figure S6 in Data S1).

Vessel–tissue contact fractions differed significantly between tissues and across species, more so than tissue fractions (Table S2 in Data S1, Figure 3b). The largest contact fraction was between vessels

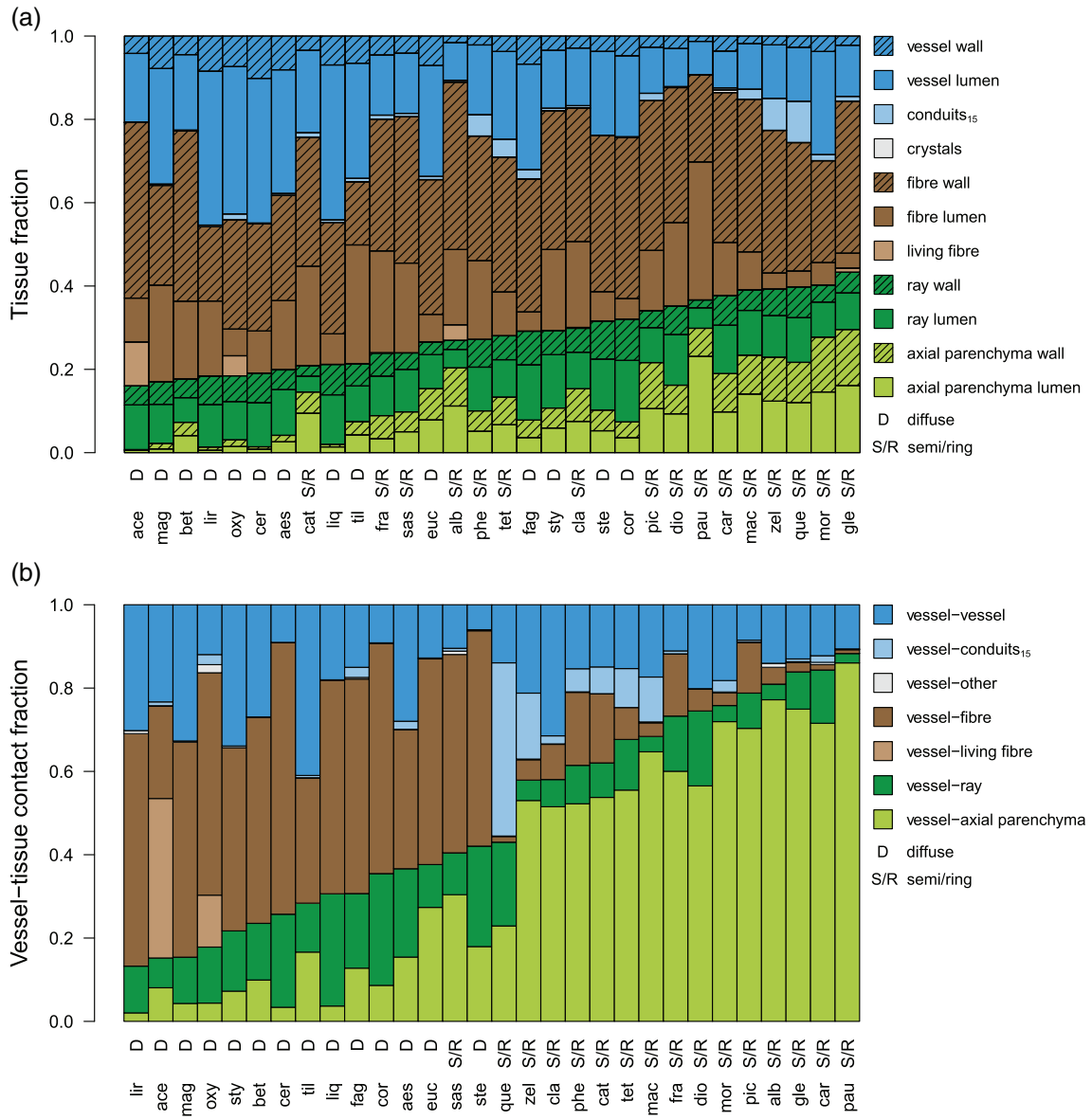

FIGURE 3 Tissue fractions sorted along increasing axial+ray parenchyma fraction (a) and vessel–tissue contact fractions sorted along increasing vessel–axial+ray parenchyma contact fraction (b) of all species examined in this study (n = 30). Three-letter codes indicate different species (Table 1). "D" denotes diffuse-porous and "S/R," semi/ring-porous species [Colour figure can be viewed at wileyonlinelibrary.com]

and axial parenchyma (0.36 ± 0.28) and between vessels and fibres (0.27 ± 0.22). Vessel–vessel contact fraction was on average 0.18 ± 0.09, followed by vessel–ray contact (0.13 ± 0.07).

Mean vessel diameter was 33 ± 7 μm (mean vessel area: 1077 ± 531 μm^2) and D_H was 61 ± 25 μm. Vessel number per mm^2 ranged from 37 to 625 (mean: 247 ± 198).

Anatomical characteristics differed considerably between diffuse-porous and semi/ring-porous species. Diffuse-porous species had higher vessel lumen fraction, vessel number per mm^2, vessel–fibre contact fraction and lower axial parenchyma fraction, vessel–axial parenchyma contact fraction, mean vessel diameter and D_H in comparison with semi/ring-porous species (Figure 4).

Wood density averaged at 0.53 ± 0.1 g cm^{-3} and ranged from 0.32 to 0.71.

3.3 | Relationships between day capacitance, anatomy and wood density

Across all species, WD and $VWC_{L\text{-}pd}$ were the strongest predictors of day capacitance. Species with higher day capacitance tended to have lower WD (r^2 = .35, p < .001, Figure 5a) and higher $VWC_{L\text{-}pd}$ (r^2 = .29, p < .01, Figure 5b). Tissue lumen fractions were not correlated with day capacitance except for a weak positive relationship with vessel lumen fraction (r^2 = .14, p < .05, Figure 5c,d).

Together, WD and $VWC_{L\text{-}pd}$ explained 44% of the variation in day capacitance (r^2_{adj} = .44, p < .001, Table 3), meaning that for a given WD, species with higher $VWC_{L\text{-}pd}$, had higher day capacitance. Adding tissue lumen fractions to this model did not improve its strength but adding contact fractions did (Table 3). For a given $VWC_{L\text{-}pd}$ and WD, day

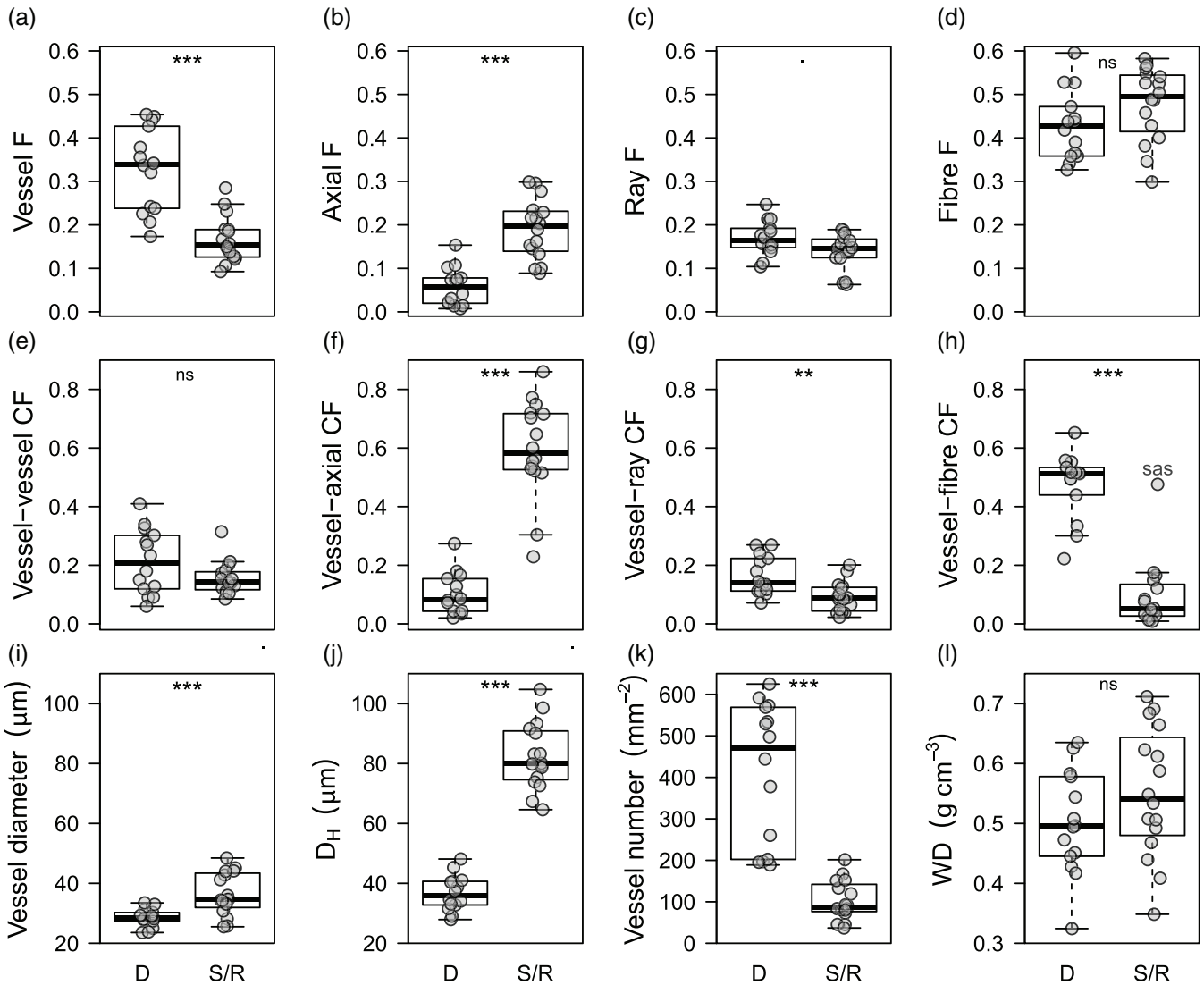

FIGURE 4 Boxplots illustrating the differences between diffuse-porous (D, n = 14) and semi/ring-porous (S/R, n = 16) species. Symbols denote species means (n = 3). Traits shown: tissue fractions (F, a–d), vessel–tissue contact fractions (CF, e–h), mean vessel diameter (i), hydraulically weighted vessel diameter (D_H, j), vessel number per area (k) and wood density (WD, l). An outlier in (h) is *Sassafras albidum* (sas). Means of the two porosity groups were compared using t-test and Wilcoxon test, and the asterisks indicate statistical significance levels: "***"p < .001, "**"p < .01, "*"p < .05, "." p < .1, "ns" p > .1

capacitance was higher in species with higher vessel–axial parenchyma contact fraction (r^2_{adj} = .56, p < .001), lower vessel–fibre contact fraction (r^2_{adj} = .54, p < .001) and lower vessel–ray contact fraction (r^2_{adj} = .54, p < .001, Table 3). These were the strongest models describing correlates of day capacitance across all species.

Relationships between day capacitance and other traits differed between porosity types. Among diffuse-porous species, WD or $VWC_{L\text{-}pd}$ were not or were only marginally correlated with day capacitance (Table 3). The trait combination that was most strongly related to day capacitance was $VWC_{L\text{-}pd}$ minus vessel–ray contact fraction (r^2_{adj} = .52, p < .01). In semi/ring-porous species, $VWC_{L\text{-}pd}$ together with WD explained the largest proportion of day capacitance variation (r^2_{adj} = .59, p < .01, or after excluding *Sassafras albidum*, r^2_{adj} = .73, p < .001; *S. albidum* was the only species with large portions of

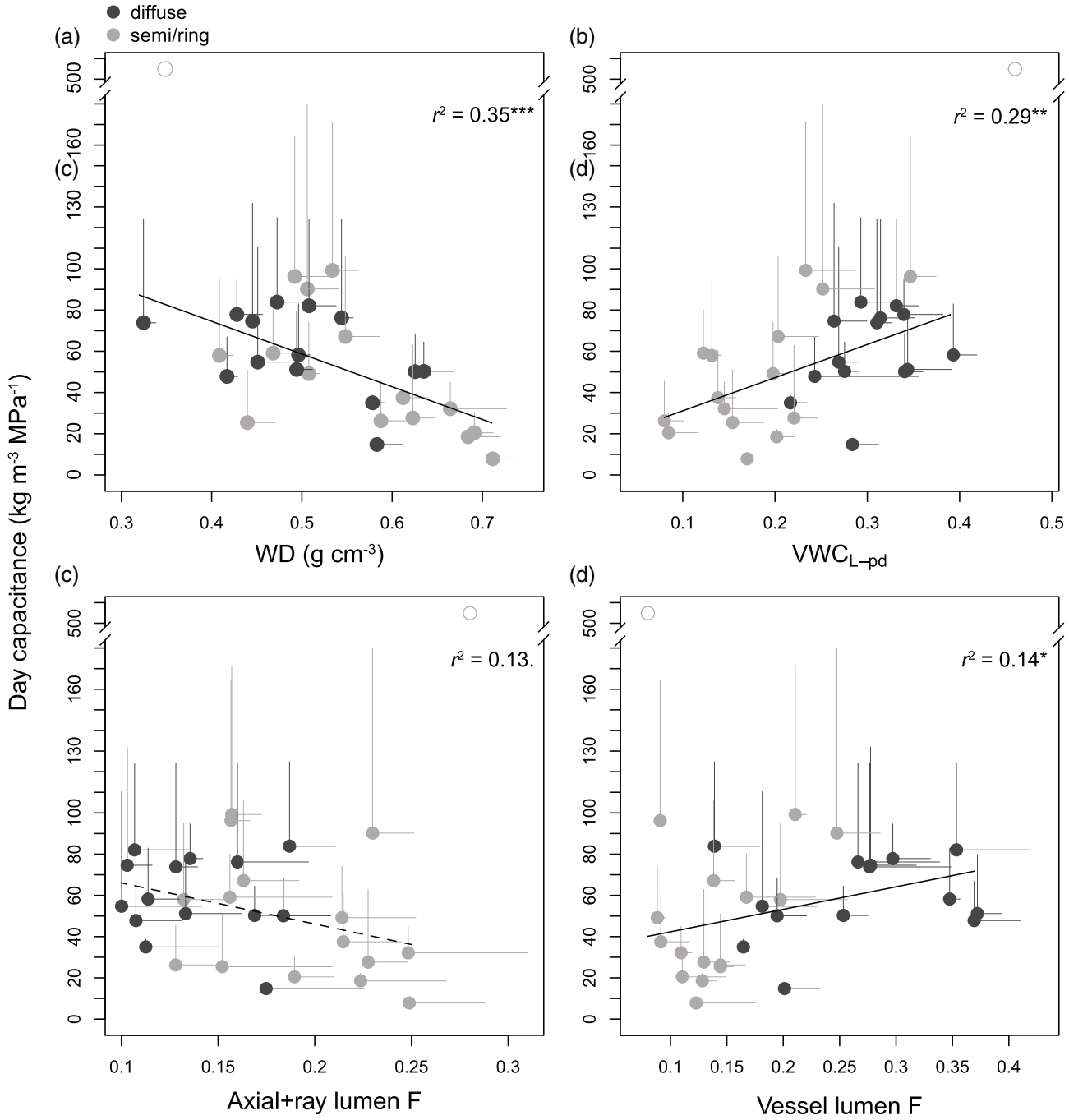

FIGURE 5 Relationships between day capacitance and: wood density (WD, a), predawn lumen volumetric water content ($VWC_{L\text{-}pd}$, b), axial +ray parenchyma lumen fraction (c), and vessel lumen fraction (d). Symbols correspond to species means (n = 3). Error bars denote one *SD*. Porosity types are reported in the legend. Fitted lines and r^2 values are shown for statistically significant relationships (solid line: p < .05, dashed line: p < .1) across all species (n = 29). Open symbol: *P. tomentosa* (excluded from the regression analyses). F: fraction. "***" p < .001, "**" p < .01, "*" p < .05, "." p < .1

TABLE 3 Best models predicting wood day capacitance, based on r^2 (bivariate) or r^2_{adj} (multiple)

Species group	Model rank	Model predicting capacitance	r^2/ r^2_{adj}	*p*
		Bivariate		
All species	1	- WD***	0.35	.001
	2	+ VWCL-pd**	0.29	.003
Diffuse	1	- average vessel area*	0.30	.041
	2	- WD.	0.25	.069
Ring/semi-ring	1	+ VWCL-pd**	0.41	.010
	2	- WD*	0.37	.016
		VWCL-pd + WD		
All species	na	+ VWCL-pd* - WD**	0.44	.000
Diffuse	na	+ VWCL-pdns - WD.	0.23	.095
Ring/semi-ring	na	+ VWCL-pd** - WD*	**0.59**	.002
		VWCL-pd + WD + tissue fractions		
All species	1	+ VWCL-pd** - WD** + axial lumen fractionns	0.47	.000
	2	+ VWCL-pd** - WD* - ray lumen fractionns	0.46	.000
	3	+ VWCL-pd** - WD* - vessel lumen fractionns	0.43	.001
		VWCL-pd + WD + contact fractions		
All species	1	+ VWCL-pd*** - WD*** + vessel–axial contact fraction**	**0.56**	.000
	2	+ VWCL-pd*** - WD*** - vessel–fibre contact fraction*	**0.54**	.000
	3	+ VWCL-pd** - WD** - vessel–ray contact fraction*	**0.54**	.000
		VWCL-pd + tissue fractions		
All species	1	+ VWCL-pd*** + fibre lumen fraction. - ray lumen fraction.	0.42	.001
	2	+ VWCL-pd*** + fibre lumen fraction** + axial lumen fractionns	0.40	.001
	3	+ VWCL-pd*** + fibre lumen fraction*	0.38	.001
Diffuse	1	+ VWCL-pd. + fibre lumen fraction.	0.25	.081
Ring/semi-ring	1	+ VWCL-pd** + vessel lumen fraction*	**0.55**	.003
	2	+ VWCL-pd** - axial+ray lumen fraction*	**0.55**	.003
	3	+ VWCL-pd** + fibre lumen fraction.	**0.50**	.006
		VWCL-pd + contact fractions		
All species	1	+ VWCL-pd*** + vessel–vessel contact fraction* + vessel–axial contact fraction*	0.42	.001
	2	+ VWCL-pd*** - vessel–ray contact fraction*	0.41	.000
	3	+ VWCL-pd*** + vessel–vessel contact fraction.	0.32	.003
Diffuse	1	+ VWCL-pd** - vessel–ray contact fraction**	**0.52**	.007
	2	+ VWCL-pd* + vessel–vessel contact fraction*	0.41	.022
Ring/semi-ring	1	+ VWCL-pd** + vessel–fibre contact fraction*	**0.62**	.002
		VWCL-pd + tissue fractions + contact fractions		
All species	1	+ VWCL-pd*** + fibre lumen fraction* - vessel–ray contact fraction*	**0.50**	.000
	2	+ VWCL-pd*** + fibre lumen fraction** + vessel–axial contact fraction*	0.48	.000
	3	+ VWCL-pd*** + fibre lumen fraction** - vessel–fibre contact fraction*	0.47	.000

Note: The three best-fit models (with $p < .1$) for each species group are shown. For all species ($n = 29$, excluding *P. tomentosa*), we allowed a maximum of three explanatory variables, and for diffuse-porous ($n = 14$) and semi/ring-porous ($n = 15$) species, we allowed a maximum of two explanatory variables, to avoid model overfitting. One outlier was removed (*S. albidum*, see Figure 4h) from the models including vessel–fibre contact fraction among semi/ring-porous species. Description of the modelling approach is in "Materials and Methods." axial: axial parenchyma. Bold: r^2 or $r^2_{adj} > .5$, regular: r^2 or $r^2_{adj} < .5$, grey: r^2 or $r^2_{adj} < .4$.
Abbreviations: $VWC_{L\text{-}pd}$, lumen volumetric water content at predawn; WD, wood density.
Significance levels: "***" $p < .001$, "**" $p < .01$, "*" $p < .05$, "." $p < .1$, "ns" $p > .1$.

gelatinous fibres and an outlier in vessel–fibre contact fraction, Figure 4h). In addition, per given $VWC_{L\text{-}pd}$, species with higher vessel–fibre contact fraction also had higher day capacitance (r^2_{adj} = .63, p < .01) but only after removing *S. albidum*.

When we substituted $VWC_{L\text{-}pd}$ with RWC_{pd} in the models listed in Table 3, their strength was either comparable ('RWC_{pd} + WD' model across diffuse-porous species), weaker by 2–7%, or not statistically significant. We also ran a set of models substituting $VWC_{L\text{-}pd}$ with WD, but none of these alternative models surpassed models including $VWC_{L\text{-}pd}$ (0.28 < r^2_{adj} < .37, p < .01). Among diffuse-porous species, none of the models were significant (p > .15), whereas across semi/ring-porous species only WD was statistically significant predictor.

Species with higher day capacitance tended to have less negative Ψ_{md} (r^2 = .39, p < .001) and narrower $\Delta\Psi_{pd\text{-}md}$ (r^2 = .45, p < .001).

The amount of water released between predawn and midday ($\Delta CWR_{pd\text{-}md}$) was positively correlated with $VWC_{L\text{-}pd}$ (r^2 = .24, p < .01). Tissue lumen fractions or vessel–tissue contact fractions were not related to $\Delta CWR_{pd\text{-}md}$, except for a weak positive correlation with vessel lumen fraction (r^2 = .21, p < .05) driven by the difference in vessel lumen fraction between the two porosity groups.

3.4 | Relationships between water storage, anatomy and wood density

Across all species, $VWC_{L\text{-}pd}$ was positively correlated with vessel lumen fraction (r^2 = .39, p < .001, Figure 6a) and negatively with axial parenchyma lumen fraction (r^2 = .18, p < .05). Other tissue lumen fractions were either weakly correlated or not correlated with $VWC_{L\text{-}pd}$ (Figure 6b,c). $VWC_{L\text{-}pd}$ tended to be higher in species with smaller vessels (log10 mean vessel area: r^2 = .44, p < .001; log10 D_H: r^2 = .48, p < .001). $VWC_{L\text{-}pd}$ was only marginally negatively correlated with WD (r^2 = .12, p < .1, Figure 6d) across all species. Within the two porosity groups, neither tissue lumen fractions nor WD were correlated with $VWC_{L\text{-}pd}$. Relationships between $RWC_{L\text{-}pd}$ and tissue fractions were somewhat different than for $VWC_{L\text{-}pd}$, and are presented in the Supporting Information (Notes S3 and Figure S7 in Data S1).

Bivariate correlations for major measured traits are reported in Figures S8 and S9 in Data S1.

4 | DISCUSSION

4.1 | Day capacitance and its structural correlates

Across all species, WD and $VWC_{L\text{-}pd}$ were most strongly and negatively correlated with day capacitance (Table 3, Figure 5a,b). An inverse relationship between WD and capacitance was also found in other studies, using the bagged leaf/shoot method (Li et al., 2018; Wolfe & Kursar, 2015), as well as in studies using psychrometers, across a wide range of water potentials (Jupa et al., 2016; Meinzer et al., 2003, 2008; Richards et al., 2014; Santiago et al., 2018; F. G. Scholz et al., 2007; Siddiq et al., 2019; Trifilò et al., 2015). Our results provide additional evidence that the native water content of stems is associated with day capacitance.

The finding that higher water content (here $VWC_{L\text{-}pd}$) is necessary to achieve high day capacitance is new, but also intuitive, that is, the more water there is, the more water can potentially be released. Perhaps less intuitive is the result that WD was a stronger driver of day capacitance than the proportions of any individual tissues. This implies that day capacitance is an emergent property of the whole wood, rather than being linked strongly to any one anatomical component. All cells in wood are tightly packed (Figure 1), in contrast to leaves, and joined via highly lignified lamellae. Therefore, any change in cell volume, resulting from water release, would require a coordinated change across neighbouring cells (Holbrook, 1995). This, presumably, would be more feasible in lower WD species that have a greater whole-organ ability to shrink (Irvine & Grace, 1997). This shrinkage would result from cell volume change due to water release and/or cell wall shrinkage due to adhesive forces between water and the surfaces of the water transporting conduits (Rosner, Karlsson, Konnerth, & Hansmann, 2009). Indeed, daily sapwood shrinkage has been observed in several angiosperm trees (Hölttä et al., 2018; Lintunen, Lindfors, Nikinmaa, & Hölttä, 2017; F. C. Scholz et al., 2008; Sevanto, Hölttä, & Holbrook, 2011), although F. C. Scholz et al. (2008) found no correlation between WD and diurnal sapwood shrinkage across six species. The latter study, however, encompassed a narrow WD range (~0.42–0.62 g cm^{-3}) and when lower density tissues from bark were included, strong covariation with capacitance was observed. Enlarging the number of species and broadening the wood density range in future studies would likely help to clarify this issue.

Parenchyma lumen fraction, as well as all other tissue lumen fractions, either were not correlated with day capacitance or were less strongly correlated than WD (e.g., vessel lumen fraction, Figure 5a,c, d). Furthermore, the tissue fractions that were significant in multiple regression models were also correlated with WD (fibre lumen and axial+ray parenchyma lumen fractions, but not vessel lumen fraction, see below). This finding is in concordance with previous studies, which, using psychrometers, also found no relationship between parenchyma fraction and capacitance in four (Jupa et al., 2016) and nine angiosperm species (Pratt, Jacobsen, Ewers, & Davis, 2007). Wood parenchyma is often assumed to be a reservoir of capacitance water (Bittencourt, Pereira, & Oliveira, 2016; Li et al., 2018; Meinzer et al., 2003; Morris et al., 2016; Plavcová & Jansen, 2015; Rungwattana & Hietz, 2018; Santiago et al., 2018; Steppe & Lemeur, 2007; Vergeynst et al., 2015) with some studies suggesting that more abundant parenchyma confers higher capacitance (Borchert & Pockman, 2005; Nardini et al., 2018; Pratt & Jacobsen, 2017; F. G. Scholz et al., 2011; Secchi et al., 2017). Here, we show that parenchyma lumen fraction does not limit capacitance (Figure 5c, Table 3). If anything, vessel lumen fraction had the strongest (albeit weaker than WD), link to day capacitance (r^2 = .14, p < .05, Figure 5d) and $\Delta CWR_{pd\text{-}md}$ (r^2 = .21, p < .05) across all species, as well as within semi/ring-porous species (multiple regression, r^2_{adj} = .55, p < .01, Table 3). This result aligns with the idea that

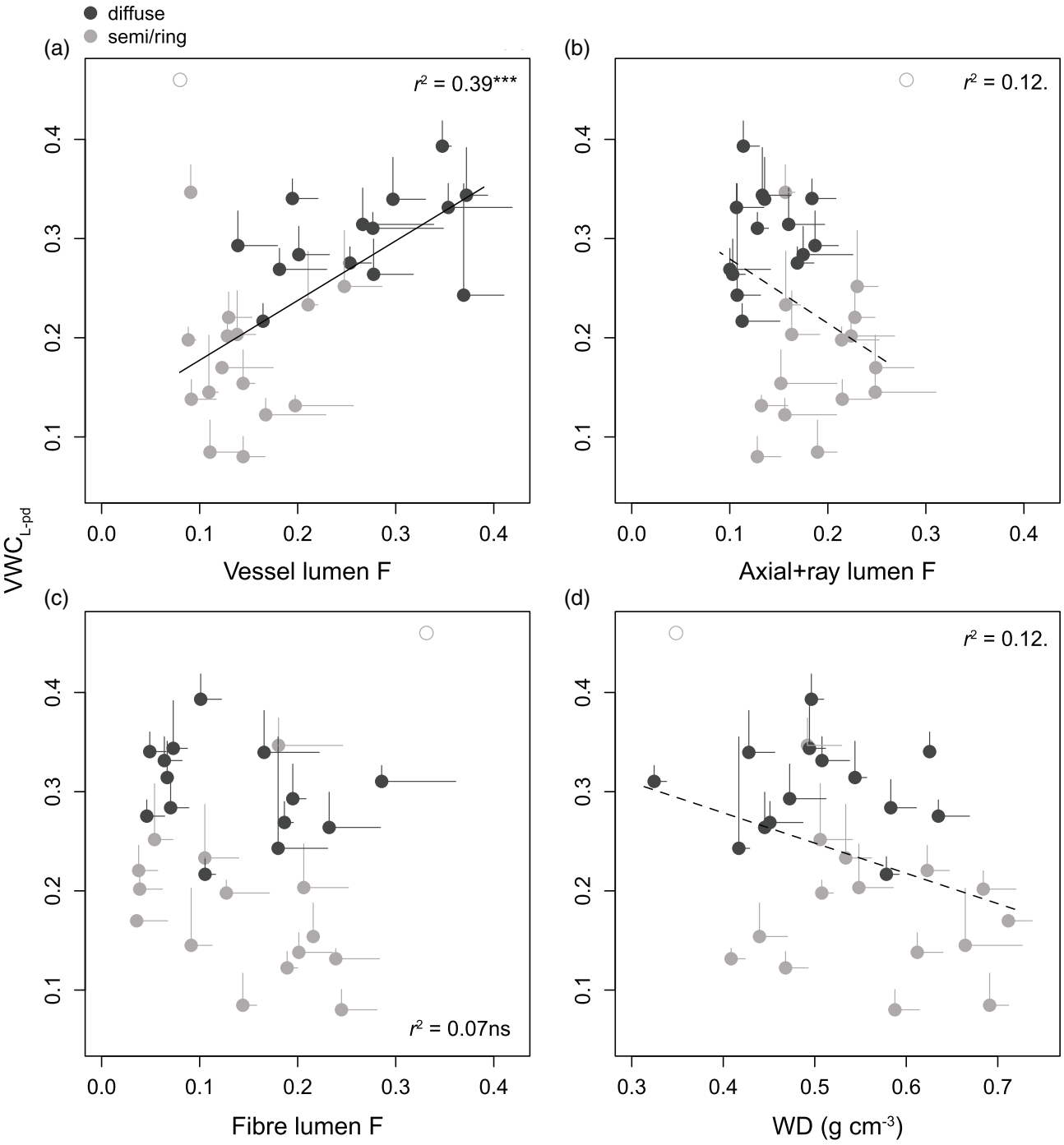

FIGURE 6 Relationships between predawn lumen volumetric water content (VWC_{L-pd}) and vessel lumen fraction (a), axial + ray parenchyma lumen fraction (b), fibre lumen fraction (c) and wood density (WD, d). Symbols correspond to species means (n = 3). Error bars denote one *SD*. Porosity types are reported in the legend. Fitted lines and r^2 values are shown for statistically significant relationships (solid line: $p < .05$, dashed line: $p < .1$) across all species (n = 29). Open symbol: *P. tomentosa* (excluded from the regression analyses). F: fraction. "***" $p < .001$, "." $p < 0.1$, "ns" not significant

cavitating vessels might contribute to capacitance, even at xylem water potentials well above critical thresholds (Hölttä, Cochard, Nikinmaa, & Mencuccini, 2009; Knipfer et al., 2019; Vergeynst et al., 2015; Yazaki et al., 2020). Moreover, $\Delta VWC_{L-pd-md}$ averaged at 0.04 ± 0.02, which is small in comparison with tissue lumen fractions (Figure 3a, Table S2 in Data S1), suggesting that lumen fraction might not limit water release or that water could be released from multiple tissues simultaneously. The interpretation of these results is further complicated by the possibility of variable water distribution across growth rings as well as within growth rings, as documented in previous studies (Umebayashi et al., 2008, 2010; Utsumi, Sano, Fujikawa, Funada, & Ohtani, 1998; Utsumi, Sano, Ohtani, & Fujikawa, 1996).

More sophisticated methods, for example, micro-computed tomography (microCT) or magnetic resonance imaging (MRI) would be necessary to resolve these questions (Fukuda et al., 2015; Knipfer et al., 2019; Yazaki et al., 2020).

Instead of tissue lumen fractions, vessel–tissue contact fractions tended to be more strongly linked to day capacitance (as independent variables in multiple regression models) across all species, as well as within porosity groups. Within semi/ring-porous species, per given $VWC_{L\text{-}pd}$, day capacitance increased with higher vessel–fibre contact fraction (Table 3), suggesting that water may be drawn from fibres into vessels in these species, as well as released from cavitating vessels (see above). This is in agreement with microCT evidence of emptying fibres (and vessels) as water potential decreases (Knipfer et al., 2017, 2019; Yazaki et al., 2020). An interesting path forward would be to measure the size of fibre lumina and taper, because these characteristics could have an additional effect on capillary water release as capillary tension and lumen diameter are negatively correlated (Hölttä et al., 2009; Tyree & Yang, 1990).

Across diffuse-porous species, per given $VWC_{L\text{-}pd,}$ day capacitance decreased with higher vessel–ray contact fraction (Table 3). Furthermore, across all species, vessel–axial (positive), vessel–fibre (negative) and vessel–ray (negative) contact fractions were all linked to day capacitance with similar strength (Table 3). Because the three contact fractions are correlated with each other (Figures S8 and S9 in Data S1), it is not possible to decipher which one of these models may represent a mechanistic link. Nevertheless, the vessel–ray contact influence is consistent across all species and within the diffuse-porous species (Table 3). How could the inverse influence of vessel–ray contact fraction on capacitance be explained? One possibility is that water is released from bark and/or pith (and transported via rays) in species that have limited *wood* capacitance (Cochard, Forestier, & Améglio, 2001; Goldstein, Meinzer, & Monasterio, 1984; Mason Earles et al., 2016; Pfautsch, Hölttä, & Mencuccini, 2015; Pfautsch, Renard, Tjoelker, & Salih, 2015). If this is true, then higher vessel–ray contact would potentially facilitate the transport and release of this water into vessels. Partitioning capacitance between bark, wood and pith could possibly clarify our understanding of whole-stem capacitance and the role of vessel–ray contact fraction.

Alternatively, there could be a mechanistic link between day capacitance and vessel–axial parenchyma contact fraction (positive relationship in our study). MicroCT studies showed that water can be released at points of contact between axial parenchyma (or fibres and vessels; Knipfer, Cuneo, Brodersen, & McElrone, 2016; Brodersen, Knipfer, & McElrone, 2018). Other investigations have shown increased molecular activity at the interface of parenchyma and vessels suggesting that parenchyma may export solutes into vessels, thus creating a solute gradient between vessels and neighbouring cells, which would drive water influx to the vessels from the surrounding tissues (Pagliarani et al., 2019; Secchi et al., 2017; Secchi & Zwieniecki, 2011). Although these studies investigated water movement from storage into embolized vessels, perhaps it is not implausible that similar water release routes could be used in day capacitance. Altogether, the different lines of evidence suggest axial and ray parenchyma may function as "gatekeepers" of water influx, but not necessarily as the main storage reservoir.

4.2 | The magnitude of capacitance and water storage

None of the studied species were fully saturated at predawn. About half of the cell lumen was empty (mean $RWC_{L\text{-}pd}$: 0.52 ± 0.17, Figure 2b). Similar values were reported in the trunk wood of three temperate angiosperms (Longuetaud et al., 2016, 2017). Other studies have estimated the proportion of wood occupied by gas to range between 0.18 (0.01–0.50) in tropical angiosperms to 0.26 (0.07–0.40) in temperate angiosperms (Gartner et al., 2004; Poorter, 2008). These and our results illustrate that considerable portions of wood are devoid of water and instead filled with gas. The water content values observed here and previously may seem dangerously low. For example, Rosner, Heinze, Savi, and Dalla-Salda (2019) reported as much as ~80% conductivity loss at ~0.65 RWC, which is the mean RWC_{pd} in our study. However, in temperate species water is not distributed evenly throughout all growth rings nor within a growth ring. In ring-porous species, the most recent one or two rings may transport the bulk of water, whereas the innermost rings, having only small vessels, may transport little water or no water at all. In contrast to this, diffuse-porous species typically have more conductive growth rings, but also a heterogeneous distribution of conductive vessels within each growth ring (Bush, Hultine, Sperry, & Ehleringer, 2010; Chaney & Kozlowski, 1977; Ellmore & Ewers, 1986; Gebauer, Horna, & Leuschner, 2008; Granier et al., 1994; Umebayashi et al., 2008, 2010; Utsumi et al., 1996, 1998). Therefore, the RWC of conductive growth rings or within-ring regions may be markedly different from the whole wood. We suggest that identifying the conductive portions of sapwood would improve our understanding of structure–function relationships.

Lack of saturation may explain why our day capacitance values are lower, sometimes by an order of magnitude, than capacitance estimated as the initial slope of the water release curve (on saturated samples) in several studies of tropical (Carrasco et al., 2015; Meinzer et al., 2003, 2008; Santiago et al., 2018) and temperate species (Jupa et al., 2016), but similar in range to Cerrado species (F. G. Scholz et al., 2007). Additionally, given that most of these studies measured capacitance on short xylem segments, it is possible that water may have been released from open conduits, thus resulting in an overestimation of capacitance (Jupa et al., 2016; Tyree & Yang, 1990). Our values overlap more so with studies which used the bagged leaf method on tropical species (Wolfe & Kursar, 2015; Zhang et al., 2013). Note that Zhang et al. (2013) measured capacitance on entire stems, including bark and pith, which may explain the presence of species with high capacitance in that study. Our results also overlap with capacitance values of Australian angiosperms, estimated from excised material using psychrometers within the native operating shoot water potential range of these species (Richards et al., 2014), as well as with capacitance values estimated from the second, "flatter"

phase of the water release curve (Jupa et al., 2016). Overall, these and previous findings highlight the importance of *in natura* water content when evaluating capacitance and the need to compare the methods used to measure capacitance.

$VWC_{L\text{-}pd}$ was more strongly correlated with day capacitance than total VWC_{pd} (wall+lumen) or the more commonly measured RWC, suggesting that absolute, lumen-based water indices are more relevant for day capacitance than relative ones. Moreover, we estimated that the amount of wall-bound water was considerable ($VWC_{W\text{-}pd}$ mean: 0.16 ± 0.03) in comparison with lumen water content ($VWC_{L\text{-}pd}$ average: 0.25 ± 0.09, Figure 2a). Although, these estimates may include some error associated with our assumptions (i.e., $M_{FSP} = 1.3 * M_D$), which has been questioned previously (Dlouhá et al., 2018; Kellogg & Wangaard, 1969), our findings highlight the need to better understand the mechanistic linkages between capacitance and the different sources of water in wood tissues.

WD, a direct outcome of total lumen and wall fractions, was weakly or not related to fresh water content indices (Figure 6d and Figure S7d in Data S1), similar to previous studies of tropical and temperate angiosperms, representing a combined total of 573 species (Kenzo, Sano, Yoneda, & Chann, 2017; Kenzo, Tomoaki, Yuta, Joseph Jawa, & Sophal, 2016; Longuetaud et al., 2016, 2017; E. Suzuki, 1999). The lack of correlation between WD and water content in these and our studies may have resulted from a large portion of the lumen fraction being filled with gas instead of water (see earlier paragraph about water and gas contents). These results caution against interpretation of WD as a direct proxy of water content and capacitance *in natura*.

4.3 | Functional significance of wood porosity types

Anatomical differences between diffuse-porous and semi/ring-porous species were significant, not only in vessel properties, as has been documented before (e.g., Davis, Sperry, & Hacke, 1999; Jupa, Doubková, & Gloser, 2019; McCulloh et al., 2010; Yang, Wang, Zhang, Bradshaw, & Hao, 2020), but also in tissue fractions and vessel–tissue contact fractions. To our knowledge, this has not been reported previously with high anatomical detail and across a considerable number of species (but see Fujiwara, Sameshima, Kuroda, & Takamura, 1991; Fujiwara, 1992; Jupa et al., 2019). What could be functional consequences of these anatomical differences between porosity groups?

Here, day capacitance did not significantly differ between diffuse-porous and semi/ring-porous species ($p = .22$, excluding *P. tomentosa*) but capacitance–trait relationships did, implying potentially different mechanisms of water release, as discussed above. Apart from capacitance, the porosity-related anatomical differences may also affect other wood functions, and we discuss these below. We focus on differences in tissue fractions and vessel–tissue contact fractions as these are the most novel results.

What could be the costs and benefits of higher parenchyma fraction in ring-porous species than in diffuse-porous? This difference could simply be a consequence of competition for space that would allow optimal water conductivity. Diffuse-porous species have small vessels and, consequently, small per-vessel conductivity. Yet, they may increase overall xylem conductivity by increasing vessel fraction (via higher vessel number per area). This rise in vessel fraction and the necessity to keep fibre fraction large enough to maintain mechanical stability, would necessarily result in lower parenchyma fraction. This tradeoff would likely be less important for ring-porous species because they have wide and efficient vessels and, consequently, they do not require high vessel fraction (Figure 4a).

Larger parenchyma fraction reflects larger capacity to store non-structural carbohydrates (NSC, Plavcová, Hoch, Morris, Ghiasi, & Jansen, 2016). We might therefore expect larger NSC pools in ring-porous species, and that these additional carbohydrate reserves could supply the carbon and energy required for new wood growth in the spring (Barbaroux, Bréda, & Dufrêne, 2003; Bréda & Granier, 1996). Available evidence implies that ring-porous species have lower ability to recover from previous year embolism than diffuse-porous species (Améglio, Bodet, Lacointe & Cochard 2002, Cochard et al., 2001; Hacke & Sauter, 1996), and thus must build new wood before or concurrently with new leaves development (M. Suzuki, Yoda, & Suzuki, 1996; Takahashi, Okada, & Nobuchi, 2013, 2015); while diffuse-porous species may use photosynthates from new leaves for wood growth. Indeed, larger drops in stem NSC content were observed in spring in several ring-porous than in diffuse-porous species (Barbaroux & Bréda, 2002; Furze et al., 2019).

Large vessel–axial parenchyma contact fraction could facilitate embolism refilling. As mentioned earlier, recent molecular (Pagliarani et al., 2019; Secchi & Zwieniecki, 2011) and microCT (Brodersen et al., 2018; Knipfer et al., 2016) studies have implied the role of parenchyma in refilling of embolized vessels. And although water could be drawn from any dead tissue (fibres, vessels or tracheids) in contact with an embolized vessel or connected to it via parenchyma cells, the amount of vessel–axial parenchyma contact fraction may determine the rate of the solute influx and the success of the refilling process. Potentially, refilling would be more beneficial in ring-porous species with large vessels. A comparison between ring-porous oak and diffuse-porous maple showed that cavitated vessels in oak were regularly refilled overnight, whereas in maple, cavitated vessels were not refilled (Taneda & Sperry, 2008). Ray parenchyma, on the other hand, runs radially, connecting bark with the inner parts of wood, and may possibly transport water, osmotically-active solutes, and other resources, thus facilitating conduit refilling (Nardini, Lo Gullo, & Salleo, 2011). However, given that there is also evidence that conduit refilling, especially in woody dicotyledons, may be rare, or even unlikely (Charrier et al., 2016; Cochard & Delzon, 2013; Sperry, 2013; J. K. Wheeler, Huggett, Tofte, Rockwell, & Holbrook, 2013), we suggest that more studies are needed to test these hypotheses.

5 | CONCLUSIONS

This work examined the anatomical correlates of twig wood water storage and day capacitance. Contrary to our expectations, tissue

lumen fractions did not constrain day capacitance. Notably, parenchyma lumen fraction was unrelated to day capacitance, challenging the common assumption that parenchyma acts as the main reservoir of capacitance water. Instead, WD, $VWC_{L\text{-}pd}$ and the connectivity between vessels and other tissues were more closely related to day capacitance than were tissue lumen fractions. Given that the fresh wood measured in this study was never saturated, we may need to rethink our interpretation of the functional and ecological relevance of capacitance estimated on saturated samples, at least in temperate species. Our understanding of wood functioning is limited by a lack of information on: (a) water distribution across and within growth rings, and (b) the combined and independent effects of wood, bark and pith. Addressing these issues would likely clarify the linkages between capacitance and the anatomical traits that are aligned with it. Notwithstanding these limitations, our findings offer new insights into capacitance and its anatomical determinants, as well as the anatomical differences between diffuse-porous and semi/ring-porous species, which all represent important avenues for future research.

ACKNOWLEDGMENTS

K.Z. and E.R. were supported by the Arnold Arboretum of Harvard University through the Postdoctoral Putnam Fellowship and the DaRin Butz Foundation Research Internship Program, respectively. We are grateful to all the Arnold Arboretum staff, and especially: Faye Rosin (Director of Research Facilitation), Living Collections, Horticulture, and the admin staff for excellent help and support. We also would like to thank the Holbrook Lab at the Department of Organismic and Evolutionary Biology of Harvard University for discussions about capacitance, providing a pressure chamber and a sliding microtome.

CONFLICT OF INTEREST

The authors declare no conflict of interest.

AUTHOR CONTRIBUTIONS

Kasia Ziemińska: Designed the study. Sean M. Gleason and Noel M. Holbrook: Contributed to concept and method development. Kasia Ziemińska: Carried out fieldwork and lab measurements. Kasia Ziemińska and Emily Rosa: Performed anatomical analysis. Kasia Ziemińska: Analysed the data and wrote first draft of the manuscript. All authors contributed to subsequent draft revisions.

ORCID

Kasia Ziemińska https://orcid.org/0000-0001-7750-4758
Sean M. Gleason https://orcid.org/0000-0002-5607-4741

REFERENCES

Améglio, T., Bodet, C., Lacointe, A., & Cochard, H. (2002). Winter embolism, mechanisms of xylem hydraulic conductivity recovery and springtime growth patterns in walnut and peach trees. *Tree Physiology*, *22*, 1211–1220.

Barbaroux, C., & Bréda, N. (2002). Contrasting distribution and seasonal dynamics of carbohydrate reserves in stem wood of adult ring-porous sessile oak and diffuse-porous beech trees. *Tree Physiology*, *22*, 1201–1210.

Barbaroux, C., Bréda, N., & Dufrêne, E. (2003). Distribution of above-ground and below-ground carbohydrate reserves in adult trees of two contrasting broad-leaved species (*Quercus petraea* and *Fagus sylvatica*). *New Phytologist*, *157*, 605–615.

Begg, J. E., & Turner, N. C. (1970). Water potential gradients in field tobacco. *Plant Physiology*, *46*, 343–346.

Bittencourt, P. R. L., Pereira, L., & Oliveira, R. S. (2016). On xylem hydraulic efficiencies, wood space-use and the safety–efficiency tradeoff. *New Phytologist*, *211*, 1152–1155.

Blackman, C. J., Pfautsch, S., Choat, B., Delzon, S., Gleason, S. M., & Duursma, R. A. (2016). Toward an index of desiccation time to tree mortality under drought. *Plant, Cell & Environment*, *39*, 2342–2345.

Borchert, R., & Pockman, W. T. (2005). Water storage capacitance and xylem tension in isolated branches of temperate and tropical trees. *Tree Physiology*, *25*, 457–466.

Bréda, N., & Granier, A. (1996). Intra- and interannual variations of transpiration, leaf area index and radial growth of a sessile oak stand (*Quercus petraea*). *Annales des Sciences Forestières*, *53*, 521–536.

Brodersen, C. R., Knipfer, T., & McElrone, A. J. (2018). In vivo visualization of the final stages of xylem vessel refilling in grapevine (*Vitis vinifera*) stems. *New Phytologist*, *217*, 117–126.

Bush, S. E., Hultine, K. R., Sperry, J. S., & Ehleringer, J. R. (2010). Calibration of thermal dissipation sap flow probes for ring- and diffuse-porous trees. *Tree Physiology*, *30*, 1545–1554.

Carrasco, L. O., Bucci, S. J., Francescantonio, D. D., Lezcano, O. A., Campanello, P. I., Scholz, F. G., … Goldstein, G. (2015). Water storage dynamics in the main stem of subtropical tree species differing in wood density, growth rate and life history traits. *Tree Physiology*, *35*, 354–365.

Chaney, W. R., & Kozlowski, T. T. (1977). Patterns of water movement in intact and excised stems of *Fraxinus americana* and *Acer saccharum* seedlings. *Annals of Botany*, *41*, 1093–1100.

Chapotin, S. M., Razanameharizaka, J. H., & Holbrook, N. M. (2006a). Baobab trees (*Adansonia*) in Madagascar use stored water to flush new leaves but not to support stomatal opening before the rainy season. *New Phytologist*, *169*, 549–559.

Chapotin, S. M., Razanameharizaka, J. H., & Holbrook, N. M. (2006b). Water relations of baobab trees (*Adansonia* spp. L.) during the rainy season: Does stem water buffer daily water deficits? *Plant, Cell & Environment*, *29*, 1021–1032.

Charrier, G., Torres-Ruiz, J. M., Badel, E., Burlett, R., Choat, B., Cochard, H., … Delzon, S. (2016). Evidence for hydraulic vulnerability segmentation and lack of xylem refilling under tension. *Plant Physiology*, *172*, 1657–1668.

Christoffersen, B. O., Gloor, M., Fauset, S., Fyllas, N. M., Galbraith, D. R., Baker, T. R., … Meir, P. (2016). Linking hydraulic traits to tropical forest function in a size-structured and trait-driven model (TFS v.1-Hydro). *Geoscientific Model Development; Katlenburg-Lindau*, *9*, 4227–4255.

Clearwater, M. J., & Meinzer, F. C. (2001). Relationships between hydraulic architecture and leaf photosynthetic capacity in nitrogen-fertilized *Eucalyptus grandis* trees. *Tree Physiology*, *21*, 683–690.

Cochard, H., & Delzon, S. (2013). Hydraulic failure and repair are not routine in trees. *Annals of Forest Science*, *70*, 659–661.

Cochard, H., Forestier, S., & Améglio, T. (2001). A new validation of the Scholander pressure chamber technique based on stem diameter variations. *Journal of Experimental Botany*, *52*, 1361–1365.

Davis, S. D., Sperry, J. S., & Hacke, U. G. (1999). The relationship between xylem conduit diameter and cavitation caused by freezing. *American Journal of Botany*, *86*, 1367–1372.

Dlouhá, J., Alméras, T., Beauchêne, J., Clair, B., & Fournier, M. (2018). Biophysical dependences among functional wood traits. *Functional Ecology*, *32*, 2652–2665.

Ellmore, G. S., & Ewers, F. W. (1986). Fluid flow in the outermost xylem increment of a ring-porous tree, *Ulmus Americana*. *American Journal of Botany*, *73*, 1771–1774.

Fox, J., & Weisberg, S. (2011). *An R companion to applied regression* (2nd ed.). Thousand Oaks, CA: Sage.

Fujiwara, S. (1992). Anatomy and properties of Japanese hardwoods II. Variation of dimensions of ray cells and their relation to basic density. *IAWA Bulletin n.s.*, *13*, 397–402.

Fujiwara, S., Sameshima, K., Kuroda, K., & Takamura, N. (1991). Anatomy and properties of Japanese hardwoods. I. Variation of fibre dimensions and tissue proportions and their relation to basic density. *IAWA Bulletin n.s.*, *12*, 419–424.

Fukuda, K., Kawaguchi, D., Aihara, T., Ogasa, M. Y., Miki, N. H., Haishi, T., & Umebayashi, T. (2015). Vulnerability to cavitation differs between current-year and older xylem: Non-destructive observation with a compact magnetic resonance imaging system of two deciduous diffuse-porous species. *Plant, Cell & Environment*, *38*, 2508–2518.

Furze, M. E., Huggett, B. A., Aubrecht, D. M., Stolz, C. D., Carbone, M. S., & Richardson, A. D. (2019). Whole-tree nonstructural carbohydrate storage and seasonal dynamics in five temperate species. *New Phytologist*, *221*, 1466–1477.

Gartner, B., Moore, J., & Gardiner, B. (2004). Gas in stems: Abundance and potential consequences for tree biomechanics. *Tree Physiology*, *24*, 1239–1250.

Gebauer, T., Horna, V., & Leuschner, C. (2008). Variability in radial sap flux density patterns and sapwood area among seven co-occurring temperate broad-leaved tree species. *Tree Physiology*, *28*, 1821–1830.

Gleason, S. M., Blackman, C. J., Cook, A. M., Laws, C. A., & Westoby, M. (2014). Whole-plant capacitance, embolism resistance and slow transpiration rates all contribute to longer desiccation times in woody angiosperms from arid and wet habitats. *Tree Physiology*, *34*, 275–284.

Goldstein, G., Andrade, J. L., Meinzer, F. C., Holbrook, N. M., Cavelier, J., Jackson, P., & Celis, A. (1998). Stem water storage and diurnal patterns of water use in tropical forest canopy trees. *Plant, Cell & Environment*, *21*, 397–406.

Goldstein, G., Meinzer, F., & Monasterio, M. (1984). The role of capacitance in the water balance of Andean giant rosette species. *Plant, Cell & Environment*, *7*, 179–186.

Granier, A., Anfodillo, T., Sabatti, M., Cochard, H., Dreyer, E., Tomasi, M., … Bréda, N. (1994). Axial and radial water flow in the trunks of oak trees: A quantitative and qualitative analysis. *Tree Physiology*, *14*, 1383–1396.

Hacke, U., & Sauter, J.J. (1996). Xylem dysfunction during winter and recovery of hydraulic conductivity in diffuse-porous and ring-porous trees. *Oecologia*, *105*, 435–439.

Hao, G.-Y., Wheeler, J. K., Holbrook, N. M., & Goldstein, G. (2013). Investigating xylem embolism formation, refilling and water storage in tree trunks using frequency domain reflectometry. *Journal of Experimental Botany*, *64*, 2321–2332.

Holbrook, N. M. (1995). Stem water storage. In B.L. Gartner (ed.), *Plant stems: Physiology and functional morphology*, (pp. 151–174). San Diego: Academic Press.

Holbrook, N. M., & Sinclair, T. R. (1992). Water balance in the arborescent palm, *Sabal palmetto*. II. Transpiration and stem water storage. *Plant, Cell & Environment*, *15*, 401–409.

Hölttä, T., Carrasco, M. D. R. D., Salmon, Y., Aalto, J., Vanhatalo, A., Bäck, J., & Lintunen, A. (2018). Water relations in silver birch during springtime: How is sap pressurised? *Plant Biology*, *20*, 834–847.

Hölttä, T., Cochard, H., Nikinmaa, E., & Mencuccini, M. (2009). Capacitive effect of cavitation in xylem conduits: Results from a dynamic model. *Plant, Cell & Environment*, *32*, 10–21.

IAWA Committee. (1989). IAWA list of microscopic features for hardwood identification. *IAWA Bulletin n.s.*, *10*, 219–332.

InsideWood. (2004). *Published on the Internet*. Retrieved from http://insidewood.lib.ncsu.edu

Irvine, J., & Grace, J. (1997). Continuous measurements of water tensions in the xylem of trees based on the elastic properties of wood. *Planta*, *202*, 455–461.

Jupa, R., Doubková, P., & Gloser, V. (2019). Ion-mediated increases in xylem hydraulic conductivity: Seasonal differences between coexisting ring- and diffuse-porous temperate tree species. *Tree Physiology*, *39*, 1313–1328.

Jupa, R., Plavcová, L., Gloser, V., & Jansen, S. (2016). Linking xylem water storage with anatomical parameters in five temperate tree species. *Tree Physiology*, *36*, 756–769.

Kabacoff, R. (2015). *R in action: Data analysis and graphics with R*. Shelter Island, NY: Manning Publications.

Kellogg, R., & Wangaard, F. (1969). Variation in the cell-wall density of wood. *Wood and Fiber Science*, *1*, 180–204.

Kenzo, T., Sano, M., Yoneda, R., & Chann, S. (2017). Comparison of wood density and water content between dry evergreen and dry deciduous forest trees in Central Cambodia. *Japan Agricultural Research Quarterly*, *51*, 363–374.

Kenzo T., Tomoaki I., Yuta I., Joseph Jawa, K., & Sophal, C. (2016). *Wood density and water content in diverse species from lowland dipterocarp rainforest and dry dipterocarp forest*. Paper presented at Proceedings of the Symposium "Frontier in Tropical Forest Research: Progress in Joint Projects between the Forest Department Sarawak and the Japan Research Consortium for Tropical Forests in Sarawak (pp. 94–103).

Knipfer, T., Cuneo, I. F., Brodersen, C. R., & McElrone, A. J. (2016). In situ visualization of the dynamics in xylem embolism formation and removal in the absence of root pressure: A study on excised grapevine stems. *Plant Physiology*, *171*, 1024–1036.

Knipfer, T., Cuneo, I. F., Earles, J. M., Reyes, C., Brodersen, C. R., & McElrone, A. J. (2017). Storage compartments for capillary water rarely refill in an intact woody plant. *Plant Physiology*, *175*, 1649–1660.

Knipfer, T., Reyes, C., Earles, J. M., Berry, Z. C., Johnson, D., Brodersen, C. R., & McElrone, A. J. (2019). Spatiotemporal coupling of vessel cavitation and discharge of stored xylem water in a tree sapling. *Plant Physiology*, *179*, 1658–1668.

Kobayashi, Y., & Tanaka, T. (2001). Water flow and hydraulic characteristics of Japanese red pine and oak trees. *Hydrological Processes*, *15*, 1731–1750.

Köcher, P., Horna, V., & Leuschner, C. (2013). Stem water storage in five coexisting temperate broad-leaved tree species: Significance, temporal dynamics and dependence on tree functional traits. *Tree Physiology*, *33*, 817–832.

Lachenbruch, B., & McCulloh, K. A. (2014). Traits, properties, and performance: How woody plants combine hydraulic and mechanical functions in a cell, tissue, or whole plant. *New Phytologist*, *204*, 747–764.

Li, X., Blackman, C. J., Choat, B., Duursma, R. A., Rymer, P. D., Medlyn, B. E., & Tissue, D. T. (2018). Tree hydraulic traits are coordinated and strongly linked to climate-of-origin across a rainfall gradient. *Plant, Cell & Environment*, *41*, 646–660.

Lintunen, A., Lindfors, L., Nikinmaa, E., & Hölttä, T. (2017). Xylem diameter changes during osmotic stress, desiccation and freezing in *Pinus sylvestris* and *Populus tremula*. *Tree Physiology*, *37*, 491–500.

Longuetaud, F., Mothe, F., Fournier, M., Dlouha, J., Santenoise, P., & Deleuze, C. (2016). Within-stem maps of wood density and water content for characterization of species: A case study on three hardwood and two softwood species. *Annals of Forest Science*, *73*, 601–614.

Longuetaud, F., Mothe, F., Santenoise, P., Diop, N., Dlouha, J., Fournier, M., & Deleuze, C. (2017). Patterns of within-stem variations in wood specific gravity and water content for five temperate tree species. *Annals of Forest Science*, *74*, 64.

Mason Earles, J., Sperling, O., Silva, L. C. R., McElrone, A. J., Brodersen, C. R., North, M. P., & Zwieniecki, M. A. (2016). Bark water uptake promotes localized hydraulic recovery in coastal redwood crown. *Plant, Cell & Environment*, *39*, 320–328.

McCulloh, K., Sperry, J. S., Lachenbruch, B., Meinzer, F. C., Reich, P. B., & Voelker, S. (2010). Moving water well: Comparing hydraulic efficiency in twigs and trunks of coniferous, ring-porous, and diffuse-porous

saplings from temperate and tropical forests. *New Phytologist*, *186*, 439–450.

McCulloh, K. A., Johnson, D. M., Meinzer, F. C., Voelker, S. L., Lachenbruch, B., & Domec, J.-C. (2012). Hydraulic architecture of two species differing in wood density: Opposing strategies in co-occurring tropical pioneer trees. *Plant, Cell & Environment*, *35*, 116–125.

Meinzer, F. C., Campanello, P. I., Domec, J.-C., Gatti, M. G., Goldstein, G., Villalobos-Vega, R., & Woodruff, D. R. (2008). Constraints on physiological function associated with branch architecture and wood density in tropical forest trees. *Tree Physiology*, *28*, 1609–1617.

Meinzer, F. C., James, S. A., & Goldstein, G. (2004). Dynamics of transpiration, sap flow and use of stored water in tropical forest canopy trees. *Tree Physiology*, *24*, 901–909.

Meinzer, F. C., James, S. A., Goldstein, G., & Woodruff, D. (2003). Whole-tree water transport scales with sapwood capacitance in tropical forest canopy trees. *Plant, Cell & Environment*, *26*, 1147–1155.

Meinzer, F. C., Johnson, D. M., Lachenbruch, B., McCulloh, K. A., & Woodruff, D. R. (2009). Xylem hydraulic safety margins in woody plants: Coordination of stomatal control of xylem tension with hydraulic capacitance. *Functional Ecology*, *23*, 922–930.

Morris, H., Plavcová, L., Cvecko, P., Fichtler, E., Gillingham, M. A. F., Martínez-Cabrera, H. I., … Jansen, S. (2016). A global analysis of parenchyma tissue fractions in secondary xylem of seed plants. *New Phytologist*, *209*, 1553–1565.

Nardini, A., Lo Gullo, M. A., & Salleo, S. (2011). Refilling embolized xylem conduits: Is it a matter of phloem unloading? *Plant Science*, *180*, 604–611.

Nardini, A., Savi, T., Trifilò, P., & Lo Gullo, M. A. (2018). Drought stress and the recovery from xylem embolism in woody plants. In F. M. Cánovas, U. Lüttge, & R. Matyssek (Eds.), *Progress in botany Progress in botany* (Vol. 79, pp. 197–231). Cham, Switzerland: Springer International Publishing.

Pagliarani, C., Casolo, V., Ashofteh Beiragi, M., Cavalletto, S., Siciliano, I., Schubert, A., … Secchi, F. (2019). Priming xylem for stress recovery depends on coordinated activity of sugar metabolic pathways and changes in xylem sap pH. *Plant, Cell & Environment*, *42*, 1775–1787.

Pfautsch, S., Hölttä, T., & Mencuccini, M. (2015). Hydraulic functioning of tree stems—Fusing ray anatomy, radial transfer and capacitance. *Tree Physiology*, *35*, 706–722.

Pfautsch, S., Renard, J., Tjoelker, M. G., & Salih, A. (2015). Phloem as capacitor: Radial transfer of water into xylem of tree stems occurs via symplastic transport in ray parenchyma. *Plant Physiology*, *167*, 963–971.

Phillips, N. G., Ryan, M. G., Bond, B. J., McDowell, N. G., Hinckley, T. M., & Čermák, J. (2003). Reliance on stored water increases with tree size in three species in the Pacific Northwest. *Tree Physiology*, *23*, 237–245.

Plavcová, L., Hoch, G., Morris, H., Ghiasi, S., & Jansen, S. (2016). The amount of parenchyma and living fibers affects storage of nonstructural carbohydrates in young stems and roots of temperate trees. *American Journal of Botany*, *103*, 603–612.

Plavcová, L., & Jansen, S. (2015). The role of xylem parenchyma in the storage and utilization of nonstructural carbohydrates. In U. Hacke (ed.), *Functional and ecological xylem anatomy* (pp. 209–234). Cham: Springer.

Poorter, L. (2008). The relationships of wood-, gas- and water fractions of tree stems to performance and life history variation in tropical trees. *Annals of Botany*, *102*, 367–375.

Pratt, R. B., & Jacobsen, A. L. (2017). Conflicting demands on angiosperm xylem: Tradeoffs among storage, transport and biomechanics. *Plant, Cell & Environment*, *40*, 897–913.

Pratt, R. B., Jacobsen, A. L., Ewers, F. W., & Davis, S. D. (2007). Relationships among xylem transport, biomechanics and storage in stems and roots of nine Rhamnaceae species of the California chaparral. *New Phytologist*, *174*, 787–798.

R Core Team. (2018). *R: A language and environment for statistical computing*. Vienna, Austria: R Foundation for Statistical Computing.

Richards, A. E., Wright, I. J., Lenz, T. I., & Zanne, A. E. (2014). Sapwood capacitance is greater in evergreen sclerophyll species growing in high compared to low-rainfall environments. *Functional Ecology*, *28*, 734–744.

Rosner, S., Heinze, B., Savi, T., & Dalla-Salda, G. (2019). Prediction of hydraulic conductivity loss from relative water loss: New insights into water storage of tree stems and branches. *Physiologia Plantarum*, *165*, 843–854.

Rosner, S., Karlsson, B., Konnerth, J., & Hansmann, C. (2009). Shrinkage processes in standard-size Norway spruce wood specimens with different vulnerability to cavitation. *Tree Physiology*, *29*, 1419–1431.

Ross, R. J. (Ed.). (2010). *Wood handbook: Wood as an engineering material* (Centennial ed.). Madison, WI: US Department of Agriculture. USDA Forest Service. Forest Products Laboratory, USA.

Rungwattana, K., & Hietz, P. (2018). Radial variation of wood functional traits reflect size-related adaptations of tree mechanics and hydraulics. *Functional Ecology*, *32*, 260–272.

Salomón, R. L., Limousin, J.-M., Ourcival, J.-M., Rodríguez-Calcerrada, J., & Steppe, K. (2017). Stem hydraulic capacitance decreases with drought stress: Implications for modelling tree hydraulics in the Mediterranean oak *Quercus ilex*. *Plant, Cell & Environment*, *40*, 1379–1391.

Santiago, L. S., Guzman, M. E. D., Baraloto, C., Vogenberg, J. E., Brodie, M., Hérault, B., … Bonal, D. (2018). Coordination and trade-offs among hydraulic safety, efficiency and drought avoidance traits in Amazonian rainforest canopy tree species. *New Phytologist*, *218*, 1015–1024.

Schneider, C. A., Rasband, W. S., & Eliceiri, K. W. (2012). NIH image to ImageJ: 25 years of image analysis. *Nature Methods*, *9*, 671–675.

Scholz, F. C., Bucci, S. J., Goldstein, G., Meinzer, F. C., Franco, A. C., & Miralles-Wilhelm, F. (2008). Temporal dynamics of stem expansion and contraction in savanna trees: Withdrawal and recharge of stored water. *Tree Physiology*, *28*, 469–480.

Scholz, F. G., Bucci, S. J., Goldstein, G., Meinzer, F. C., Franco, A. C., & Miralles-Wilhelm, F. (2007). Biophysical properties and functional significance of stem water storage tissues in Neotropical savanna trees. *Plant, Cell & Environment*, *30*, 236–248.

Scholz, F. G., Phillips, N. G., Bucci, S. J., Meinzer, F. C., & Goldstein, G. (2011). Hydraulic capacitance: Biophysics and functional significance of internal water sources in relation to tree size. In F. C. Meinzer, B. Lachenbruch, & T. E. Dawson (Eds.), *Size- and age-related changes in tree structure and function Tree physiology* (pp. 341–361). Dordrecht, the Netherlands: Springer.

Secchi, F., Pagliarani, C., & Zwieniecki, M. A. (2017). The functional role of xylem parenchyma cells and aquaporins during recovery from severe water stress. *Plant, Cell & Environment*, *40*, 858–871.

Secchi, F., & Zwieniecki, M. A. (2011). Sensing embolism in xylem vessels: The role of sucrose as a trigger for refilling. *Plant, Cell & Environment*, *34*, 514–524.

Sevanto, S., Hölttä, T., & Holbrook, N. M. (2011). Effects of the hydraulic coupling between xylem and phloem on diurnal phloem diameter variation: Xylem-phloem hydraulic coupling and phloem diameter variation. *Plant, Cell & Environment*, *34*, 690–703.

Siddiq, Z., Zhang, Y.-J., Zhu, S.-D., & Cao, K.-F. (2019). Canopy water status and photosynthesis of tropical trees are associated with trunk sapwood hydraulic properties. *Plant Physiology and Biochemistry*, *139*, 724–730.

Sperry, J. (2013). Cutting-edge research or cutting-edge artefact? An overdue control experiment complicates the xylem refilling story. *Plant, Cell & Environment*, *36*, 1916–1918.

Sperry, J. S., Nichols, K. L., Sullivan, J. E. M., & Eastlack, S. E. (1994). Xylem embolism in ring-porous, diffuse-porous, and coniferous trees of Northern Utah and Interior Alaska. *Ecology*, *75*, 1736–1752.

Steppe, K., & Lemeur, R. (2007). Effects of ring-porous and diffuse-porous stem wood anatomy on the hydraulic parameters used in a water flow and storage model. *Tree Physiology*, *27*, 43–52.

Suzuki, E. (1999). Diversity in specific gravity and water content of wood among Bornean tropical rainforest trees. *Ecological Research*, *14*, 211–224.

Suzuki, M., Yoda, K., & Suzuki, H. (1996). Phenological comparison of the onset of vessel formation between ring-porous and diffuse-porous deciduous trees in a Japanese temperate forest. *IAWA Journal*, *17*, 431–444.

Takahashi, S., Okada, N., & Nobuchi, T. (2013). Relationship between the timing of vessel formation and leaf phenology in ten ring-porous and diffuse-porous deciduous tree species. *Ecological Research*, *28*, 615–624.

Takahashi, S., Okada, N., & Nobuchi, T. (2015). Relationship between vessel porosity and leaf emergence pattern in ring- and diffuse-porous deciduous trees in a temperate hardwood forest. *Botany*, *93*, 31–39.

Taneda, H., & Sperry, J. S. (2008). A case-study of water transport in co-occurring ring- versus diffuse-porous trees: Contrasts in water-status, conducting capacity, cavitation and vessel refilling. *Tree Physiology*, *28*, 1641–1651.

Trifilò, P., Nardini, A., Gullo, M. A. L., Barbera, P. M., Savi, T., & Raimondo, F. (2015). Diurnal changes in embolism rate in nine dry forest trees: Relationships with species-specific xylem vulnerability, hydraulic strategy and wood traits. *Tree Physiology*, *35*, 694–705.

Tyree, M. T., & Yang, S. (1990). Water-storage capacity of *Thuja*, *Tsuga* and *Acer* stems measured by dehydration isotherms. *Planta*, *182*, 420–426.

Umebayashi, T., Utsumi, Y., Koga, S., Inoue, S., Fujikawa, S., Arakawa, K., … Oda, K. (2008). Conducting pathways in north temperate deciduous broadleaved trees. *IAWA Journal*, *29*, 247–263.

Umebayashi, T., Utsumi, Y., Koga, S., Inoue, S., Matsumura, J., Oda, K., … Otsuki, K. (2010). Xylem water-conducting patterns of 34 broadleaved evergreen trees in southern Japan. *Trees*, *24*, 571–583.

Utsumi, Y., Sano, Y., Fujikawa, S., Funada, R., & Ohtani, J. (1998). Visualization of cavitated vessels in winter and refilled vessels in spring in diffuse-porous trees by cryo-scanning electron microscopy. *Plant Physiology*, *117*, 1463–1471.

Utsumi, Y., Sano, Y., Ohtani, J., & Fujikawa, S. (1996). Seasonal changes in the distribution of water in the outer growth rings of *Fraxinus mandshurica* var. *Japonica*: A study by cryo-scanning electron microscopy. *IAWA Journal*, *17*, 113–124.

Vergeynst, L. L., Dierick, M., Bogaerts, J. A. N., Cnudde, V., & Steppe, K. (2015). Cavitation: A blessing in disguise? New method to establish vulnerability curves and assess hydraulic capacitance of woody tissues. *Tree Physiology*, *35*, 400–409.

Warton, D. I., Duursma, R. A., Falster, D. S., & Taskinen, S. (2012). smatr 3– An R package for estimation and inference about allometric lines. *Methods in Ecology and Evolution*, *3*, 257–259.

Wei, T., & Simko V. (2017). *R package "corrplot": Visualization of a corelation matrix (Version 0.84)*. https://github.com/taiyun/corrplot

Wheeler, E. A. (2011). InsideWood - A web resource for hardwood anatomy. *IAWA Journal*, *32*, 199–211.

Wheeler, J. K., Huggett, B. A., Tofte, A. N., Rockwell, F. E., & Holbrook, N. M. (2013). Cutting xylem under tension or supersaturated with gas can generate PLC and the appearance of rapid recovery from embolism. *Plant, Cell & Environment*, *36*, 1938–1949.

Wolfe, B. T., & Kursar, T. A. (2015). Diverse patterns of stored water use among saplings in seasonally dry tropical forests. *Oecologia*, *179*, 925–936.

Yang, D., Wang, A.-Y., Zhang, J.-L., Bradshaw, C. J. A., & Hao, G.-Y. (2020). Variation in stem xylem traits is related to differentiation of upper limits of tree species along an elevational gradient. *Forests*, *11*, 349.

Yazaki, K., Levia, D. F., Takenouchi, A., Watanabe, M., Kabeya, D., Miki, N. H., … Fukuda, K. (2020). Imperforate tracheary elements and vessels alleviate xylem tension under severe dehydration: Insights from water release curves for excised twigs of three tree species. *American Journal of Botany*, *107*, 1122–1135.

Zanne, A. E., Westoby, M., Falster, D. S., Ackerly, D. D., Loarie, S. R., Arnold, S. E. J., & Coomes, D. A. (2010). Angiosperm wood structure: Global patterns in vessel anatomy and their relation to wood density and potential conductivity. *American Journal of Botany*, *97*, 207–215.

Zhang, Y.-J., Meinzer, F. C., Qi, J.-H., Goldstein, G., & Cao, K.-F. (2013). Midday stomatal conductance is more related to stem rather than leaf water status in subtropical deciduous and evergreen broadleaf trees. *Plant, Cell & Environment*, *36*, 149–158.

Ziemińska, K., Westoby, M., & Wright, I. J. (2015). Broad anatomical variation within a narrow wood density range—A study of twig wood across 69 Australian angiosperms. *PLoS One*, *10*, e0124892.

Zimmermann, M. H. (1983). *Xylem structure and the ascent of sap*. Berlin Heidelberg: Springer-Verlag.

SUPPORTING INFORMATION

Additional supporting information may be found online in the Supporting Information section at the end of this article.

How to cite this article: Ziemińska K, Rosa E, Gleason SM, Holbrook NM. Wood day capacitance is related to water content, wood density, and anatomy across 30 temperate tree species. *Plant Cell Environ*. 2020;1–20. https://doi.org/10.1111/pce.13891